

X-ray Spectral Characteristics of GINGA Gamma-Ray Bursts

T. E. Strohmayer¹, E. E. Fenimore²

Los Alamos National Laboratory
Los Alamos, New Mexico 87545

T. Murakami

Institute of Space and Astronautical Science
1-1 Yoshinodai 3, Sagamihara, Kanagawa, 229 Japan

A. Yoshida

The Institute of Physical and Chemical Research (RIKEN)
2-1, Hirose, Wako, Saitama, 351-01, Japan

Received: _____ Accepted: _____

Abstract

We have investigated the spectral characteristics of a sample of bright γ -ray bursts detected with the γ -ray burst sensors aboard the satellite *Ginga*. This instrument employed a proportional and scintillation counter to provide sensitivity to photons in the 2 - 400 keV region and as such provided a unique opportunity to characterize the largely unexplored X-ray properties of γ -ray bursts. The photon spectra of the *Ginga* bursts are well described by a low energy slope, a bend energy, and a high energy slope. In the energy range where they can be compared, this result is consistent with burst spectral analyses obtained from the BATSE experiment aboard the *Compton Observatory*. However, below 20 keV we find evidence for a positive spectral number index in approximately 40% of our burst sample, with some evidence for a strong rolloff at lower energies in a few events. There is a correlation (Pearson's $r = -0.62$) between the low energy slope and the bend energy. We find that the distribution of spectral bend energies extends below 10 keV. There has been some concern in cosmological models of GRBs that the bend energy covers only a small dynamic range. Our result extends the observed dynamic range and, since we observe bend energies down to the limit of our instrument, perhaps observations have not yet limited the range. The *Ginga* trigger range was virtually the same as BATSE's, yet we find a different range of fit parameters. One possible explanation might be that GRBs have two break energies, one often in the 50 to 500 keV range and the other near 5 keV. Both BATSE and *Ginga* fit with only a single break energy so BATSE tends to find breaks near the center of its

¹ Current address: GSFC, stroh@pcasrv.gsfc.nasa.gov

² efenimore@lanl.gov

energy range and we tend to find breaks in our energy range. The observed ratio of energy emitted in the x-rays relative to the gamma-rays can be much larger than a few percent and, in fact, is sometimes larger than unity. The average for our 22 bursts is 24%. We also investigated spectral evolution in two bursts. In these events we find strong evidence for spectral softening as well as a correlation between photon intensity and spectral hardness. We also find that the X-ray signal below 30 keV itself softens in both of these events. There is one example of a strong x-ray excess at low energy. In addition to providing further constraints on γ -ray burst models, the description provided here of burst spectra down to 2 keV should prove useful to future planned efforts to detect bursts at X-ray energies.

Subject Headings: Gamma Rays: Bursts - X-Rays: General

1. Introduction

Twenty-five years after their discovery, γ -ray bursts continue to defy explanation. Analysis of burst energy spectra remains one of the principal methods for determining the physical processes responsible for these events. Recent analysis of spectroscopy data from the Burst and Transient Source Experiment (BATSE) on the *Compton Gamma Ray Observatory* (CGRO) has demonstrated the diversity of burst spectral continua in the $\approx 30 - 3000$ keV range (*cf.* Band *et al.* 1993; hereafter B93). However, few instruments to date have probed the X-ray regime of γ -ray bursts between 2 and 20 keV.

The first detections of X-rays in the 1-8 keV range from γ -ray bursts were reported by Wheaton *et al.* (1973), Trombka *et al.* (1974), and Metzger *et al.* (1974). Later results from the P78-1 (Laros *et al.* 1984) and *Hakucho* (Kato *et al.* 1984) satellites confirmed that γ -ray bursts often produce significant X-ray emission. In addition, these satellites provided the first evidence suggesting that the X-ray emission might outlast the main γ -ray event in some bursts (so called X-ray tails). These early data provided only modest spectral resolution in the X-ray regime, however, based on their results, the γ -ray burst detector (GBD) flown aboard the *Ginga* satellite was specifically designed to investigate burst spectra in the X-ray regime (Murakami *et al.* 1989). *Ginga* was launched in February of 1987, and the GBD was operational from March, 1987 until the reentry of the spacecraft in October, 1991. Several important results have emerged from the study of burst spectra recorded with the *Ginga* GBD. Harmonically spaced line features have been reported from several *Ginga* events (Murakami *et al.* 1988; Fenimore *et al.* 1988; Yoshida *et al.* 1992; Graziani *et al.* 1992), and have been interpreted as due to cyclotron absorption in the strong magnetic field of a neutron star. Recently, preliminary results indicate that BATSE has also detected absorption lines (Briggs *et al.*, 1997). In addition to line features, *Ginga* has observed X-ray tails in a number of bursts, as well as x-ray preactivity in one event (Yoshida *et al.* 1989; Murakami *et al.* 1991; & Murakami *et al.* 1992b). More recently, the BeppoSax satellite has observed several bursts in both x-rays and gamma-rays (Piro, *et al.* 1997) and discovered soft x-ray afterglows (Costa *et al.*, 1997). This latter discovery has opened the way for the long sought GRB counterparts, including one with a measured redshift (Metzger *et al.*, 1997). Here, we provide for 22 GRBs a compilation and description of γ -ray burst spectral continua emphasizing the X-ray spectral characteristics.

Before BATSE, the analysis of γ -ray burst spectra suggested that the continua can be fitted adequately by a range of models, with power law, optically thin thermal bremsstrahlung and thermal synchrotron formulae providing acceptable fits to many spectra (*cf.* Mazets *et al.* 1982; Matz *et al.* 1985; and Hurley 1989). Although these functional forms adequately describe many burst spectra it is not at all clear that the corresponding physical processes are responsible for the burst spectra, because spectral shapes inconsistent with

each other may often be consistent with the same data. The compilation by B93 of average spectra from a large sample of BATSE bursts provides the most detailed statistical description presently available of burst continua in the range from $\approx 30 - 3000$ keV. (Also see Schaefer *et al.* 1994.) It is our purpose here to provide an extension of this statistical description of burst spectra down to 2 keV using an analysis of bright bursts observed by the *Ginga* GBD. In addition to providing further constraints on proposed burst source models it is our hope that the information provided here will be useful to future soft X-ray experiments which will require the range of GRB spectral characteristics to estimate, for example, the expected rate of burst detections. To facilitate comparison of our results with the published BATSE spectra we adopt the same burst spectral form as described in B93. Although it does not imply any particular physical process, this form provides an adequate description of BATSE bursts and the *Ginga* bursts studied here. Given the excellent statistics generated by the BATSE detectors, the fact that the B93 shape can adequately fit the GRB spectrum is a strong argument that it should be used even though it does not imply any physical process.

We begin in §2 with a brief description of the GBD instruments, as well as a discussion of the analysis techniques employed, including a discussion of the constraints placed on us by the lack of positional information for many of the *Ginga* bursts. In §3 we describe the spectral properties of the *Ginga* sample and compare these results with the previously reported BATSE spectra. In §4 we investigate the spectral evolution of a smaller number of bright bursts. In §5 we summarize the x-ray emission relative to the gamma-ray emission. We conclude in §6 with a summary and discussion of our principal results.

2. Instrumental Summary and Data Analysis Techniques

The GBD aboard *Ginga* consisted of a proportional counter (PC) sensitive to photons in the 2-25 keV range and a scintillation counter (SC) recording photons with energies between 15-400 keV. Each detector had an ≈ 60 cm² effective area. The PC and SC provided 16 and 32 channel spectra, respectively, over their indicated energy ranges. The detectors were uncollimated except for the presence of shielding to reduce backside illumination and the mechanical support for the PC window. The field of view was effectively π steradian for both the PC and the SC. In burst mode the GBD recorded spectral data from the PC and SC at 0.5 s intervals for 16 seconds prior to the burst trigger time, and for 48 seconds after the trigger. This Memory Read Out (MRO) data was used for many of the spectral fits described here. In the event that MRO data was not available for a burst, we utilized the spectral data from the “real time” telemetry modes. For these bursts, spectral data were available with either 2, 16, or 64 second accumulations. For the longer accumulations, spectral studies were not generally feasible. See Murakami *et al.* (1989) for more information concerning the detectors.

Before a model can be fitted to the data the background spectrum must be estimated and subtracted from the counts. For a majority of the analyzed bursts a linear fit to the MRO data in each energy channel provided a reasonable fit to the pre- and post-burst data. In a few cases, a quadratic fit was used. Events with large variations in the background were rejected from this analysis. For several events, the background was estimated from real-time data which was generally available for a longer time period both before and after the event. The background subtracted spectra were then fitted using a standard χ^2 minimization technique. In this method the input model spectrum is first folded through the detector response functions, thereby providing count predictions for each energy channel, these predictions are then compared to the observed counts using a χ^2 statistic. The model parameters are adjusted iteratively until a minimum in χ^2 is obtained. As mentioned previously, we have adopted the spectral model employed by B93 because of its relative simplicity and ability to accurately characterize a wide range of spectral continua, in addition this choice facilitates direct comparison of our results with those obtained from the BATSE bursts. This model has the form

$$N(E) = A \left(\frac{E}{100\text{keV}} \right)^\alpha \exp(-E/E_0) \quad , \quad (\alpha - \beta)E_0 \geq E$$

$$N(E) = A \left[\frac{(\alpha - \beta)E_0}{100\text{keV}} \right]^{\alpha - \beta} \exp(\beta - \alpha) \left(\frac{E}{100\text{keV}} \right)^\beta \quad , \quad (\alpha - \beta)E_0 \leq E, \quad (1)$$

where A is an overall scale factor, α is the low energy spectral index, β is the high energy spectral index, and E_0 is the exponential cutoff or bend energy. In addition, to facilitate comparison with previous calculations we have restricted the ranges of β to be greater than -5.0. Recently, this spectral form has been characterized with the peak of the νF_ν distribution (i.e., E_p). The conversion is that $E_p = (\alpha + 2)E_0$.

The *Ginga* GBD was in operation from March 1987 to October 1991. During this time ≈ 120 γ -ray bursts were identified (*cf.* Ogasaka *et al.* 1991; & Fenimore *et al.* 1993). We selected from this group a sample of 22 events for which good spectral data were available and for which we could be reasonably certain that the burst occurred within the forward, π steradian field of view of the detectors (front-side events). Front-side events are easily identified because they have consistent fluxes in the energy range observed by both instruments (15 to 25 keV). This sample includes 18 of the events searched for spectral lines (Fenimore *et al.* 1993). Excluded bursts usually show strong rolloffs below 25 keV and spectral fits with an absorption component due to aluminum (a principal spacecraft material) are consistent with this interpretation. Sky positions for four of the events in our sample are known because of simultaneous detections with either BATSE or WATCH. Incidence angles into GBD for bursts 910429, 910717, and 910814 (9.3, 34.3, 37.0 degrees, respectively) were derived from knowledge of the GBD orientation at the time of the burst and the published BATSE positions (Fishman *et al.* 1994). Burst 900126 was seen by the

WATCH experiment and the incidence angle (50 degrees) was derived using the published position (Lund 1992).

For the remaining events, the incidence angle θ of the photons into the detectors is uncertain (0° equals normal incidence). Since the detector response is a function of this angle, the inferred source spectrum and thus peak intensity of these events is also somewhat uncertain. We selected 37 degrees for the incidence angle when the angle was unknown. This is a typical angle considering that the mechanical support for the window on the PC acts as a collimator limiting the field of view to an opening angle of $\sim \pm 60$ degrees. We have used Monte Carlo simulations to evaluate the impact of the unknown incidence angle. For each simulation, we selected a random incidence angle between 0 and 60 degrees. We calculated a response matrix and used it with the burst's best fit parameters in Equation (1) to generate simulated spectra. Background was added and Poisson statistics applied. We then analyzed the simulated data the same way we analyzed the burst data: an estimated background was subtracted and the best fit parameters for Equation (1) were found based on a response matrix corresponding to 37 degrees.

The uncertain incidence angle usually only affects α and E_0 in Equation (1) so we will emphasize the affect of the uncertain angle on those parameters. Figure 1 shows typical examples covering interesting values of α (i.e., positive α 's: 0.74, 0.22, and 1.67 for GB900901, GB870303, and GB900322, respectively). Each cross represents the best fit α and E_0 from a simulation. We show 100 simulations per burst for clarity although we did 10^3 simulations. The contour includes 68% of the cases (based on the 10^3 simulations). As was found by B93, the observations tend to agree with a range of solutions satisfying $\alpha \propto \log E_0$. Figure 1 shows the range of uncertainty due to both the unknown incidence angle and counting statistics.

3. X-ray Spectral Characteristics of GINGA Bursts

For each burst in the sample we selected a time interval ΔT over which to sum the counts in each spectral channel. This selection was based on the need to increase the signal to noise in the computed spectrum and the desire to constrain the spectrum near the peak of the time profile. Sometimes, ΔT is limited by the available time resolution in the real time data. If the burst has a smaller duration than our resolution, we will underestimate its intensity (e.g., GB910814). Spectra can evolve substantially during the course of an event (*cf.* Mazets *et al.* 1981; Golenetskii *et al.* 1983; Norris *et al.* 1986; Band *et al.* 1992; Kargatis *et al.* 1994; Ford *et al.* 1995; and §4). We attempted to compute a spectrum consistent with the most intense portion of each burst's time profile. For real-time events we endeavored to compute the spectra from the time ranges which encompassed the majority of the burst. We employed all spectral channels in most of the model fits except for the lowest PC channel which has extremely small effective area, for a total of 47 channels.

To illustrate these spectral fits we show in Figure 2 the best-fit spectrum and indicate the contribution of χ^2 for each channel for each burst analyzed. The burst nomenclature specifies the year/month/day on which each event was detected. In the event that more than one burst occurred on a given day, a letter is assigned to the burst according to the order of occurrence.

We choose the format of Figure 2 to simultaneously show the best-fit spectra as well as how well each spectral channel fits the observations. Note that the ordinate is spectral number flux, not counts. Let O_i be the observed net count rate for the i -th channel and M_i be the predicted net rate from the model, $N(E)$. Let σ_i^2 be the variance on O_i . The solid line in these figures is $N(E)$ and each channel is represented by a point plotted at $O_i N(E)/M_i$ with a vertical line length of $\pm \sigma_i N(E)/M_i$. Thus, for each point, the distance from the point to the line divided by the length of the error bar is $(M_i - O_i)/\sigma_i = \chi_i$, that is, it gives the contribution of the point to the total χ^2 . The alternative ways to present these data would be to plot the residuals $M_i - O_i \pm \sigma_i$ or to plot M_i and $O_i \pm \sigma_i$. Each method emphasizes a different aspect of the fitting: the model photon spectrum by the first, the residuals by the second, and the observed counts by the third. It is equally possible to visualize the contribution of each channel to χ^2 in all three presentations. All three methods are only as valid as the assumed $N(E)$. The third method is often characterized as being independent of the model but, of course, the only useful information is whether the observed counts differ significantly from the predicted counts, and those predicted counts depend on the model. One must be careful in all three presentations to avoid interpreting deviations of O_i from M_i as implying that the spectrum might be locally different from the assumed $N(E)$ because in all three cases, M_i depends on a wide range (i.e., from E to ∞) of $N(E)$ so is very model dependent. The temptation to view local differences between O_i and M_i as evidence that $N(E)$ should be different is probably strongest for our format since $N(E)$ is present in the figure. However, all three formats are equivalent on this score: the quality of a model fit should be judged solely on the basis of the total χ^2 value and not on how any one point (or group of points) matches (or mismatches) the best-fit model. Our format is misleading if one attempts to interpret the deviations as implying that the best-fit model should locally change to “agree” with the observations. That is why this format is inappropriate for presentations of absorption line candidates or to argue that a model needs to be changed. However, in this work, we are showing *acceptable* fits and we will not argue for changes in the best fit model. This format shows the best fit spectral function and how well each point agrees with it. As such, it is a good method for visualizing the low energy behavior of GRBs.

The results of the spectral fits for each burst are summarized in Table 1. Here, ΔT specifies the time interval for calculation of the spectrum, $R_{x/g}$ is the ratio of the emitted energy in x-rays relative to the gamma-rays (see §5), E_0 , α , and β are the best-fit model

parameters, and χ_r^2 is the reduced χ^2 for the fit. Each spectral fit was performed with 43 degrees of freedom, and the quoted uncertainties for β are 1σ estimates assuming one parameter of interest. The strong coupling in the B93 spectral shape between α and E_0 means that one should not quote separate confidence regions for α and E_0 (see below).

Previous spectral analyses have been reported for some of the bursts listed here, mostly with regard to the presence of lines in their spectra, but also because of interesting X-ray properties (*cf.* Murakami *et al.* 1988; Fenimore *et al.* 1988; Wang *et al.* 1989; Yoshida *et al.* 1992; Yoshida *et al.* 1989; & Murakami *et al.* 1991), here we have restricted our interest to the spectral continua of the bursts. In Table 1 we also give references to previous analyses of these bursts (last column of Table 1).

The spectral fits are generally acceptable, with χ_r^2 of order unity for most of the bursts. In agreement with B93 we find that a range in these model parameter values is required to adequately describe γ -ray burst spectra. In Figure 3 we show a graphical comparison between the BATSE results taken from B93 and our results for the *Ginga* sample. Figure 3a contains the best-fit spectra for the 22 bursts in the *Ginga* sample, while Figure 3b displays the 54 spectra computed from the BATSE data of B93. In each case the spectra are plotted only over the nominal band-pass of each instrument (2-400 keV and 20-3000 keV for *Ginga* and BATSE respectively). For BATSE, bursts were measured over slightly different bandpasses due to different detectors having different gains. See B93 for the actual measured range of each burst. The spectra have been normalized to 1.0 photon/keV at 100 keV. Between 20 and 400 keV the two samples are in substantial agreement, and span a consistent range of spectral shapes.

Of particular interest is the behavior of the *Ginga* sample at X-ray energies. About 40% of the bursts in the sample show a positive spectral number index below 20 keV (i.e., $\alpha > 0$), with the suggestion of rolloff toward lower energies in a few of the bursts (α as large as $\sim +1.5$). Unfortunately, the lack of data below 1 keV, and the often weak signal below 5-10 keV precludes us from establishing the physical process (photoelectric absorption, self-absorption) that may be involved in specific bursts. The remainder of the burst spectra continue to increase below 10 keV. Observations of the low-energy asymptote can place serious constraints on several GRB models, most notably the synchrotron shock model which predicts that α should be between $-3/2$ and $-1/2$ (Katz 1994). Crider *et al.* (1997) uses examples from BATSE to argue that some GRB violate these limits during some *time-resolved* samples. We find violations of these limit in the *time-integrated* events.

Figure 4 summarizes the low energy behavior of GRBs as a scatter plot of the bursts α 's and E_0 's. In Figure 4a, we show the 68% confidence regions for 20 of the bursts in Table 1. These confidence regions were calculated the same way as in Figure 1. For two bursts we only show the best fit parameters as solid squares because a simple power law could nearly fit the entire spectra. Note for GB881009 that α is nearly equal to β and for

GB880205, the bend energy is well above our energy range. Although we give the formal best fit parameters in Table 1, effectively, E_0 was undetermined or not necessary for the fit in those two bursts. We repeated the analysis of Figure 4a in Figure 4b except we did each simulation at the angle for which we analyzed the burst (37 degrees, in most cases). Thus, Figure 4b indicates the size of the confidence regions if we knew the incidence angle. By comparing Figure 4a and Figure 4b, we see that the lack of knowledge of the incidence angle into *Ginga* does not introduce much more uncertainty than the counting statistics. On average, because of the uncertain incidence angle, the confidence region for E_0 is 22% larger and the confidence region for α is larger by 0.06.

In Figure 4c we combine the results from this paper and B93. The open squares are the BATSE results from B93 and the solid squares are the *Ginga* results presented here. Many of the *Ginga* points lie within the range found by BATSE. However, the lowest E_0 found by BATSE was 14 keV (set, of course, by the lowest energy observed by BATSE). *Ginga* extends E_0 values down to 2 keV. BATSE had a small fraction (15%) of events with $\alpha > 0$ whereas *Ginga* has 40% of events with $\alpha > 0$. In general this is because there is a correlation between α and E_0 such that the lower energy range of *Ginga* samples a parameter space with more events with $\alpha > 0$. For the 76 points, the Pearson's r coefficient is -0.62. The formal significance is about 4σ although that ignores the complicated error bars that are caused by the fact that the observations tend to agree with a range of $\alpha - E_0$. However, the existence of a correlation seems reasonable: there are virtually no events seen by BATSE at large α , large E_0 and few low α , low E_0 events seen by *Ginga*. The error bars (Fig. 4a) are large on the *Ginga* points, but not large enough to indicate that they all should fall where the average BATSE events occurred. We note that GB900126 is an event for which we know the incidence angle. This event is important to our conclusions because it has one of the largest α 's and there is no uncertainty due to an unknown incidence angle. In Figure 4c we show a representative confidence regions for one BATSE event from B93, burst 451. We note that the confidence regions quoted in Table 4 of B93 were found separately for α and E_0 , ignoring the coupling, so are much smaller than the real confidence regions and cannot be compared to ours.

In our sample of bursts, we find that α can be both less than zero and greater than zero. Negative α 's are often seen in time-integrated BATSE spectra. Positive α 's where the spectrum rolls over at low energies are usually only seen in *time resolved* BATSE spectra (Crider et al. 1997).

The *Ginga* trigger range (50 to 400 keV) was virtually the same as BATSE's. Thus, we do not think we are sampling a different population of bursts, yet we get a different range of fit parameters. The lack of events with E_0 's between 6 and 20 keV cannot be used to support two populations because we do not have enough events. One possible explanation might be that GRBs have two break energies, one often in the 50 to 500 keV range and the

other near 5 keV. Both BATSE and *Ginga* fit with only a single break energy so BATSE tends to find breaks near the center of its energy range and we tend to find breaks in our energy range. Without good high energy observations of bursts with low E_0 , it is difficult to know whether they also have a high energy bend.

Preece et al (1996) utilized a low energy discriminator channel and detected emission in excess of what would be expected from a fit at higher energy. Preece et al (1996) report excesses in 15% of the investigated BATSE bursts. One of our bursts, GB880205, shows a clear strong excess at low energy and two other *Ginga* bursts, GB880830 and GB910418, probably also shows an excess. For GR910418, Preece et al (1996) also reported an excess. From the Preece et al (1996) result, we would expect about 3 of our bursts to show an excess so we are consistent with the BATSE result.

4. Spectral Evolution of GINGA Bursts

It was recognized shortly after the discovery of the γ -ray bursts that their spectra show significant variation within a single event (Wheaton *et al.* 1973; Metzger *et al.* 1974; Teegarden & Cline 1980; & Yoshida *et al.* 1989). Analysis of *Solar Maximum Mission*, and BATSE data indicate that burst spectra tend to evolve from hard to soft, both for individual peaks in the temporal profile, as well as over the entire course of the burst, though counter-examples to this general trend can be found (*cf.* Norris *et al.* 1986; and Band *et al.* 1992, Band, 1997, Crider *et al.* 1997). Previous analyses of the *Ginga* data identified several bursts with soft X-ray preactivity as well as X-ray tails which generally showed softer spectra than the most intense portion of the event (Murakami *et al.* 1991; and Murakami *et al.* 1992b).

Several of the *Ginga* bursts which we have analyzed were of sufficient duration and intensity to permit spectral evolution studies. Here we summarize our results for two events, bursts 901001 and 890929. Incidence angles into the detectors for these events are not known, however, when comparing spectra computed from different time intervals within the same burst, the choice of incidence angle is not important, since this angle did not vary during the event. We therefore used an angle of 37° for these calculations as well. For each burst we subdivided the time profiles into several temporal regions and then computed the best-fit spectrum for each region. We used the same GRB model (eq. [1]) as in the previous calculations.

In Figure 5a we show the time profiles for burst 901001 in five different energy ranges. The dotted vertical lines delineate the six temporal regions in which spectra were computed. Also shown is a linear estimate of the background computed from the pre- and post-burst signal. Note that the low energy, X-ray emission persists longer than the high energy emission, suggestive of overall softening of the burst spectrum (*cf.* Yoshida *et al.* 1992). In Figure 5b we show the best-fit spectra computed for each indicated time period. We

have again normalized each spectrum to 1.0 at 100 keV. The Figure legend identifies each spectrum with the time interval for which it was computed. For completeness, the best-fit model parameters computed from each time interval are also given in Table 2. Comparison of the spectra computed from the first two time intervals suggests possible initial hardening during the rise to peak intensity. After the peak there is strong evidence for softening of the spectrum. In fact, for intervals T_5 and T_6 there is still a significant signal in the PC, however, there is no evidence of corresponding emission above 100 keV in the SC. To further investigate the relationship between intensity and hardness we have computed E_p and flux F (between 2 and 400 keV) for each time interval. The resulting values are plotted in the inset panel of Figure 5b. The 1σ uncertainties were estimated from Monte Carlo simulations using the best-fit spectral parameters derived from each time interval. The direction of temporal evolution is along the solid line, from upper right to lower left. Thus, there is initial hardening during the rise to peak of the burst, followed by softening for the remainder of the event. In Figures 6a, 6b and Table 2 we show the corresponding results for burst 890929. There is also evidence for an X-ray tail in this event, and the softening of the spectrum during the course of this burst is also quite apparent, though no initial hardening during the rise to peak is evident. For these events the X-ray signal also softens in addition to the higher energy γ -rays.

The hardness-intensity plots for these two bursts suggest a correlation between hardness and intensity similar to that reported by Golenetskii *et al.* (1983) , Kargatis *et al.* (1994), and Bhat *et al.* (1994). Linear fits to the $\log E_p$ versus $\log F$ data (*i.e.* $\log E_p = a \log F + b$) for bursts 901001 and 890929 give $a \approx 0.3$. The results of our linear fits are shown in Table 3.

5. X-ray Emission Relative to Gamma-ray Emission

Early measurements of the x-rays associated with gamma-rays were fortuitous observations by collimated x-ray detectors that just happen to catch a GRB in their field of view. From a few events it appeared that the amount of energy in x-rays was only a few percent (Laros et al. 1984) confirming that GRBs were, indeed, a gamma-ray phenomena. The *Ginga* experiment was designed with a wide field of view to detect a sufficient number of events to determine the range of x-ray characteristics. Early reports from *Ginga* events indicated that sometimes a much larger fraction of the emitted energy was contained in the x-rays. For example, by comparing the signal in the proportional counter (roughly 2 to 25 keV) to that of the scintillator (roughly 15 to 400 keV), we reported an x-ray to gamma-ray emission ratio up to $\sim 46\%$ (Yoshida *et al.* 1989). Such a ratio depends on the bandpass for which it is evaluated. One can use the parameters from Table 1 in Equation (1) to determine the ratio of emission for arbitrary bandpasses. This would be useful, for example, to predict the range of emission that might be seen in instruments such as ROSAT. Here, we find the

ratio of emission for a typical x-ray bandpass (2 to 10 keV) compared to the BATSE energy range (50 to 300 keV). The ratio is defined to be $R_{x/g} = \int_2^{10} EN(E)dE / \int_{50}^{300} EN(E)dE$. This ratio is listed in the third column of Table 1. Figure 7 presents the distribution for the events analyzed in this paper. Although the ratio is often a few percent, for some events the ratio is near (or larger than) unity. Some GRBs actually have more energy in the x-ray bandpass than the gamma-ray bandpass. The simply average of the 22 values is 24%. This large value arises because of the few events with nearly equal energy in the x-ray and gamma-ray bandpass. However, even the logarithmic average is 7%.

6. Discussion and Summary

Several of the results reported here are of particular interest. There is some concern in cosmological models of GRBs that the bend energy occurs only over a small range of values implying that the bulk Lorentz factor only varies a little from burst to burst (Brainerd, 1994, 1997). The *Ginga* bursts extends the range of observed bend energies from above 500 keV (with BATSE) to ~ 3 keV (*Ginga*). This *Ginga* result implies that, perhaps, we have not yet observed the lower limit on bend energies and, thus, the range of dynamic range of bulk Lorentz factors has not been limited. Regardless, any successful model for the burst sources must be able to explain the range of bend energies.

The spectral evolution observed in bursts 901001 and 890929 support the consensus that hard to soft spectral evolution is a prevalent feature of the burst mechanism. Both *Ginga* bursts analysed here would seem to fit this scenario. Initial soft to hard evolution has been previously reported for burst 900126 (Murakami *et al.* 1991), and is also suggested by our analysis of burst 901001. Perhaps the timescale for the energization process is rapid enough in some bursts to preclude observation of the initial hardening of the spectrum.

Several future space missions have been planned with the goal of detecting bursts at soft X-ray energies. For example, the X-ray spectral distribution of γ -ray bursts has consequences for the High Energy Transient Experiment (HETE) mission (*cf.* Ricker *et al.* 1992) which has as one of its main goals the identification of burst counterparts derived from localization of bursts using X-ray observations. The initial localization of sources by HETE depends on the detection of bursts with a coded aperture X-ray instrument operating from 2 - 25 keV. Estimates of the number of bursts expected to be seen per year can be made based on the range of x-ray spectra presented here.

We have investigated the X-ray spectral characteristics of a sample of 22 bright γ -ray bursts detected by the GBD which flew aboard *Ginga*. In the energy band where they can be compared, the range of spectral shapes which describe the *Ginga* sample are consistent with those derived from analyses of bright BATSE bursts. Consistent with Preece *et al.* 1996, we find at least one event (GB880205) that has an x-ray excess relative to the GRB spectra from Equation 1. Moreover, the *Ginga* spectra extend down to ≈ 2 keV, and thus provide

a useful characterization of burst spectra over an energy range at which burst spectra have not often been measured. In addition, we have investigated spectral evolution in two longer duration events. We found evidence for spectral softening during both of these events, along with a correlation between hardness and intensity.

This work was carried out under the auspices of the US Department of Energy. It is a pleasure to acknowledge helpful discussions with Jean in 't Zand and Richard Epstein, and Tony Crider. We also thank David Band for extensive discussions on the error bars for α and E_0 as well as many comments on the manuscript. Tony Crider kindly helped with the production of Figures 5 and 6.

References

- Band, D., 1997, ApJ, in press
- Band, D. *et al.* 1992, in AIP Conference Proceedings 265, Gamma-Ray Bursts, ed. W. S. Paciesas & G. J. Fishman (New York: AIP), 169.
- Band, D., *et al.* 1993, ApJ, 413, 281.
- Bhat, P. N., *et al.* 1994, ApJ, 426, 604.
- Brainerd, J. J., 1994, Ap. J. 428, 21
- Brainerd, J. J., 1997, Ap. J. submitted.
- Briggs, et al. 1997, talks given at the Aspen and Huntsville 1997 conferences on GRBs.
- Costa, E., et al., 1997, Nature, 387, 783
- Crider, A., et al. 1997, ApJ, 479, L93
- Fenimore, E. E, *et al.* 1988, ApJ, 335, L71.
- Fenimore, E. E., *et al.* 1993, in AIP Conference Proceeding 280, Compton Gamma-Ray Observatory, ed. M. Friedlander, N. Gehrels, & D. Macomb, (New York:AIP), 917.
- Fishman, G., *et al.* 1994, ApJS, 92, 229
- Ford, L. A. *et al.* 1995, ApJ, 439, 307
- Golenetskii, S. V., *et al.* 1983, Nature, 306, 451.
- Graziani, C., 1992, in Gamma-Ray Bursts, ed. C. Ho, R. I. Epstein & E. E. Fenimore, (Cambridge: Cambridge University Press), 407.
- Hurley, K. 1989, in NATO ASI Series C, Vol. 270, Cosmic Gamma Rays, Neutrinos, and Related Astrophysics, ed. M. M. Shapiro & J. P. Wefel (Dordrecht: Kluwer), 337
- Graziani, C., 1993, in AIP Conference Proceeding 280, Compton Gamma-Ray Observatory, ed. M. Friedlander, N. Gehrels, & D. Macomb, (New York:AIP), 897.
- Kargatis, V. E., Liang, E. P., Hurley, K. C., Barat, C., Eveno, E., and Niel, M., 1994, ApJ, 422, 260.
- Katoh, M., Murakami, T., Nishimura, J., Yamagami, T., Tanaka, Y., and Tsunemi, H., 1984, in *High Energy Transients in Astrophysics*, AIP Conference Proc. No 115, ed. S. E. Woosley (AIP New York), 390.
- Katz, J. I., 1994, ApJ, 432, L107
- Laros, J. G., Evans, W. D., Fenimore, E. E., Klebesadel, R. W., Shulman, S., and Fritz, G., 1984, ApJ, 286, 681

- Lund, N., 1992, in *Gamma-Ray Bursts: Observations, Analyses and Theories*. proc. of Los Alamos Workshop, ed. C. Ho, R. Epstein, and E. Fenimore, pg. 188.
- Matz, S. M., Forrest, D. J., Vestrand, W. T., Chupp, E. L., Share, G. H., & Rieger, E., 1985, *ApJ*, 288, L37.
- Mazets, E. P., *et al.* 1981, *Astrophys. Space Sci.*, 80, 3.
- Mazets, E. P., Golenetskii, S. V., Ilyinskii, V. N., Aptekar, R. L., 1982, *Astrophys. Space Sci.*, 82, 261.
- Metzger, A. E., Parker, R. H., Gilman, D., Peterson, L. E., & Trombka, J. I., 1974, *ApJ*, 194, L19.
- Metzger, M. et al., 1997, *Nature*, 387, 878
- Murakami, T., Ogasaka, Y., Yoshida, A., & Fenimore, E. E., 1992a, in *AIP Conference Proceedings 265, Gamma-Ray Bursts*, ed. W. S. Paciesas & G. J. Fishman (New York: AIP), 28.
- Murakami, T., Inoue, H., van Paradijs, J., Fenimore, E., & Yoshida, A., 1992b, in *Gamma-Ray Bursts*, ed. C. Ho, R. I. Epstein & E. E. Fenimore, (Cambridge: Cambridge University Press), 239.
- Murakami, T. *et al.*, 1988, *Nature*, 335, 234.
- Murakami, T. *et al.*, 1989, *Publ. Astron. Soc. Jap.*, 41, 405.
- Murakami, T. *et al.*, 1991, *Nature*, 350, 592.
- Norris, J. P., *et al.* 1986, *ApJ*, 301, 213.
- Ogasaka, Y., Murakami, T., Nishimura, J., Yoshida, A. & Fenimore, E. E., 1991, *ApJ*, 383, L61.
- Owens, A. *et al.* 1994, in *Proceedings of 1993 BATSE Gamma-Ray Burst Workshop*, ed. G. J. Fishman, J. J. Brainerd, and K. Hurley, (New York: AIP), 665
- Piro, L, et al., *A&A*, in press.
- Preece, R., et al., 1996, *ApJ*, 473, 310
- Ricker, G. R. *et al.*, 1992, in, *Gamma Ray Bursts: Observations, Analyses, and Theories, Proceedings of the Los Alamos Workshop on Gamma-Ray Bursts*, (Cambridge), ed: Ho, C., Epstein, R. I., and Fenimore, E. E., p. 288
- Schaefer, B. E., *et al.* 1994, *ApJS*, 92, 285
- Teegarden, B. J., & Cline, T.L., 1980, *ApJ*, 236, L67.
- Wang, J. C. L., *et al.* 1989, *Phys. Rev. Lett.*, 63, 1550.

Wheaton, W. A., *et al.* 1973, ApJ, 185, L57.

Yoshida, A., Murakami, T., Nishimura, J., Kondo, I. & Fenimore, E. E., 1992, in Gamma-Ray Bursts, ed. C. Ho, R. I. Epstein & E. E. Fenimore, (Cambridge: Cambridge University Press), 399.

Yoshida, A., *et al.* 1989, PASJ, 41, 509.

Yoshida, A., & Murakami, T., 1994, in Proceedings of 1993 BATSE Workshop, ed. G. Fishman, J. Brainerd, & K. Hurley, (New York: AIP) pg. 333.

Figure Captions

Figure 1–Simulations for three bursts to determine the effects of the unknown incidence angle and the counting statistics. Each cross is a simulation for a burst located at an angle randomly selected between 0 and 60 degrees but analyzed with a response matrix corresponding to 37 degrees, the response matrix used to analyze the *Ginga* spectra. One hundred simulations are shown for clarity but 10^3 were used. The contour includes 68% of the events.

Figure 2–Best fit spectrum for each burst in our sample. The vertical error bars are $\pm 1\sigma$, and the distance from the photon spectrum to the center of the horizontal bar represents the residual in units of 1σ . Thus, the position of the points represent the contribution of that data point to the χ^2 of the fit (see text). The horizontal bars represent the energy loss bins.

Figure 3a–The best-fit spectra for the 22 *Ginga* bursts in our sample. Each curve has been normalized to 1.0 photons/keV at 100 keV. The spectra are plotted from 2.0 to 400.0 keV, the approximate range of sensitivity of the *Ginga* GBD.

Figure 3b–The best-fit spectra for 54 BATSE bursts. The best-fit parameters are taken from B93. We have plotted the spectra from 20.0 keV to 3 MeV, the approximate band pass for the BATSE spectral fits.

Figure 4a–Simulations to determine the 68% confidence regions of α and E_0 . The confidence regions were found in the same manner as in Figure 1 and include both the effects of the unknown incidence angle and the counting statistics. The nature of the model (eq. [1]) is such that a range of parameters satisfying $\alpha \propto \log E_0$ can be consistent with the data. For two events, E_0 was unnecessary or undetermined and they are shown as solid squares.

Figure 4b–Confidence regions reflecting the uncertainty due just to the counting statistics. For these simulations it was assumed that the incidence angle was known and the same as the analysis angle (37 degrees, for most bursts). By comparing Figure 4a and Figure 4b, we see that the effects of the uncertain incidence angle is minor compared to the effects of the counting statistics. The uncertain angle increases, on average, $\log(E_0)$ by 0.09 and α by 0.06.

Figure 4c–Low energy slopes and bend energies for *Ginga* and BATSE events. The open squares are 54 BATSE events from B93 and the solid squares are the 22 *Ginga* events reported in this paper. The *Ginga* events extend the observed range of break energies to lower values and reveal a correlation (Pearson's $r = -0.62$) between the low energy slopes

(α) and the bend energy (E_0). For comparisons with Figure 4a, we show the confidence region for one BATSE event (number 451).

Figure 5a–Time history of burst 901001 recorded in five energy bands, two from the PC and three from the SC. The dotted vertical lines denote the time intervals in which spectra were computed. The dashed line is a linear estimate of the background derived from a fit to pre- and post-burst data. To displace each profile vertically, a constant value of 600 counts has been added successively to each profile.

Figure 5b–Spectra computed from the six time intervals of burst 901001 delineated in Figure 5a. The legend indicates the time interval for which each spectrum was computed. The inset Figure shows the hardness-intensity evolution of this event. The direction of temporal evolution is along the solid line, from upper right to lower left.

Figure 6a–Time history of burst 890929 recorded in five energy bands, two from the PC and three from the SC. The dotted vertical line denote the time intervals in which spectra were computed. The dashed line is a linear estimate of the background derived from a fit to pre- and post-burst data. To displace each profile vertically, a constant value of 600 counts has been added successively to each profile.

Figure 6b–Spectra computed from the six time intervals of burst 890929 delineated in Figure 6a. The legend indicates the time interval for which each spectrum was computed. The inset Figure shows the hardness-intensity evolution of this event. The direction of temporal evolution is along the solid line, from upper right to lower left.

Figure 7–The distribution of the ratio of the energy emitted in x-rays relative to that emitted in gamma-rays. The x-ray bandpass is defined to be from 2 to 10 keV and the gamma-ray bandpass is the BATSE range of 50 to 300 keV. Note there are some examples of equal energy in the x-rays and the gamma-rays. The average ratio of the energy in the x-rays to the energy in the gamma-rays is 24%.

Table 1

Spectral fits to GINGA bursts

Burst ^a	ΔT^b	$R_{x/g}^c$	E_0^d	α^e	β^f	χ_r^2 ^g	Ref. ^h
870303	5.0	0.182	3.62	0.74	-1.63 ± 0.02	0.88	1, 3, 6, 9, 10, 11
870414	8.0	0.056	22.0	0.032	-1.80 ± 0.12	1.97	3
870521	48.0	0.923	2.38	0.82	-2.12 ± 0.04	1.47	3
870707	10.0	0.095	53.6	-0.67	-2.07 ± 0.10	1.55	3
870902	2.5	0.031	202	-0.76	-1.50 ± 0.25	1.11	3
880205	10.0	0.010	1997	-0.62	-5.0	1.49	1, 2, 3, 4, 8, 9, 15
880725	4.0	0.032	67.7	-0.32	-5.0	1.03	
880830	5.0	0.048	126	-0.75	-5.0	1.43	
881009	16.0	0.303	4.68	-1.46	-1.67 ± 0.01	1.36	
881130	3.0	0.023	34.0	0.28	-2.66 ± 0.61	1.10	
890704	3.0	0.072	43.5	-0.45	-2.05 ± 0.10	1.39	
890929	5.0	0.027	118	-0.54	-5.0	1.26	8, 9
900126	6.5	0.670	1.97	1.63	-2.05 ± 0.02	1.13	5, 7, 9, 10, 12
900221	12.0	0.043	298	-0.92	-5.0	1.51	
900322a	16.0	0.496	1.74	1.67	-1.91 ± 0.05	0.78	
900623	5.0	0.035	22.9	0.16	-1.63 ± 0.06	1.19	9
900901	64.0	1.233	3.67	0.22	-2.26 ± 0.14	1.71	
900928	3.5	0.011	106	-0.21	-5.0	1.29	
901001	5.0	0.043	120	-0.70	-5.0	1.21	
910429	32.0	0.818	4.54	-0.24	-2.08 ± 0.04	0.91	13
910717	5.0	0.017	32.1	0.27	-1.69 ± 0.06	1.33	13, 14, 16
910814	128.0	0.014	334	-0.60	-5.0	0.96	13, 14, 15, 16

^a Year/month/day of event^b Accumulation time of spectrum in sec^c ratio of the emitted energy in 2 to 10 keV relative to 50 to 300 keV (see § 5)^d Break energy for Equation 1 (in keV), uncertainties are shown in Figure 4a^e Low energy spectral index, uncertainties are shown in Figure 4a^f High energy spectral index^g Reduced χ^2 for best fit spectrum (43 dof)^h References to previous work 1: Murakami *et al.* 1988, 2: Fenimore *et al.* 1988, 3: Yoshida *et al.* 1989, 4: Wang *et al.* 1989, 5: Murakami *et al.* 1991, 6: Graziani *et al.* 1992, 7: Lund 1992, 8: Yoshida *et al.* 1992, 9: Murakami *et al.* 1992a, 10: Murakami *et al.* 1992b, 11: Graziani *et al.* 1993, 12: Yoshida & Murakami: 1994, 13: Fishman *et al.* 1994, 14: Schaefer *et al.* 1994 15: Fenimore *et al.* 1993, 16: Band *et al.* 1993, Preece *et al.* 1996.

Table 2Spectral Evolution Parameters^a

Time	A	901001		
		E_0	α	β
T_1	0.0398	122.7	-0.810	-5.00
T_2	0.1056	121.0	-0.702	-5.00
T_3	0.0295	101.5	-0.976	-5.00
T_4	0.0330	53.80	-0.898	-2.64
T_5	0.0124	108.6	-1.291	-2.57
T_6	0.0059	108.4	-1.410	-3.42

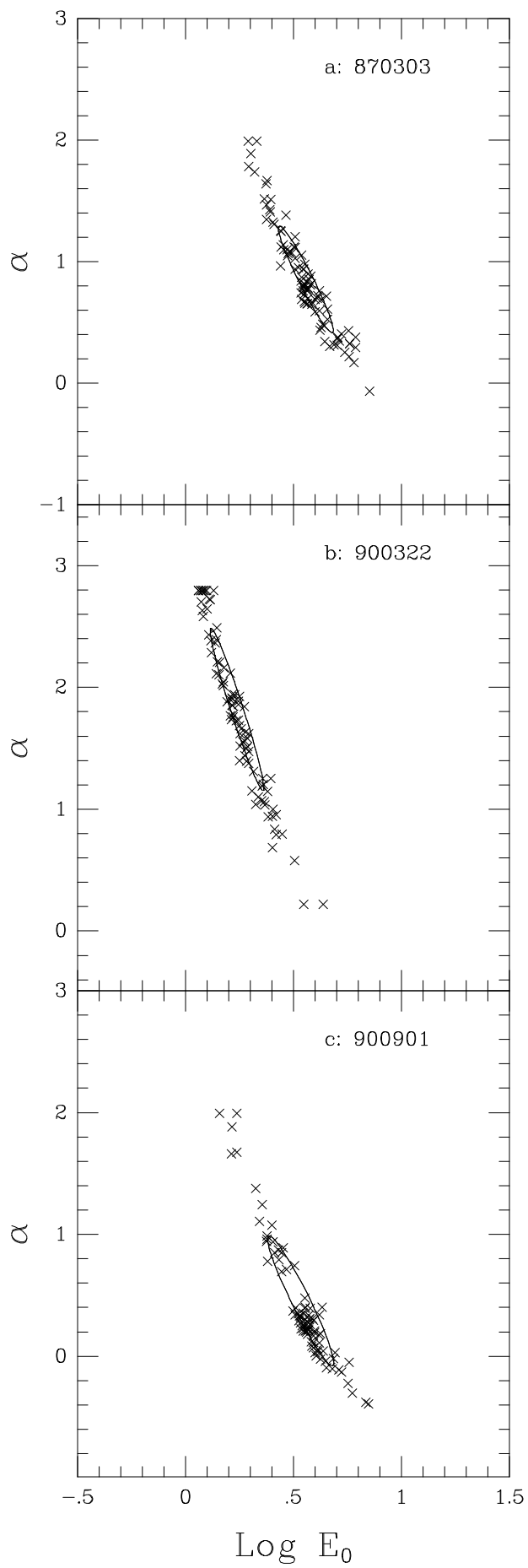
Time	A	890929		
		E_0	α	β
T_1	0.2598	118.2	0.233	-5.00
T_2	0.2334	114.9	-0.087	-5.00
T_3	0.0780	102.1	-0.565	-5.00
T_4	0.0832	52.0	-0.554	-1.80
T_5	0.1011	20.91	-0.534	-1.70
T_6	0.5743	10.29	0.134	-2.84

^a See § 2 for a discussion of the parameters.**Table 3**Hardness-Intensity Correlations^a

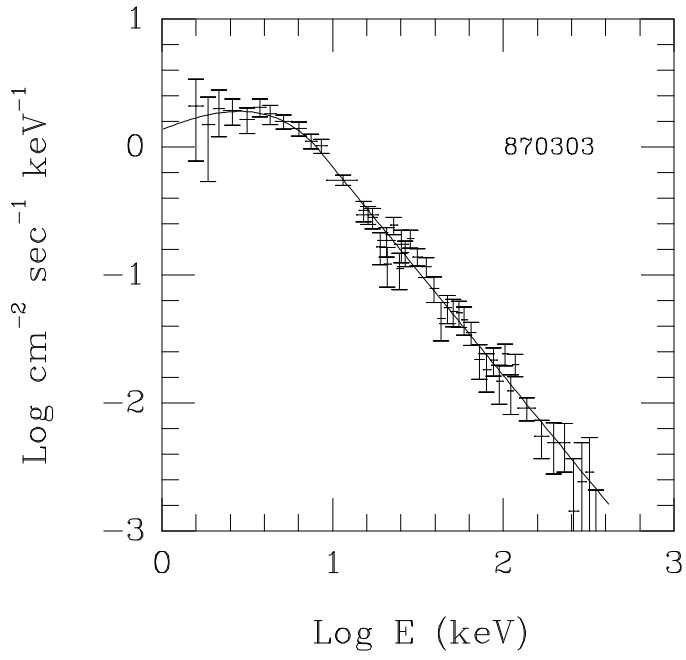
Bursts	a	σ_a	b	σ_b	P
901001	0.276	0.035	3.79	0.208	0.05
890929	0.471	0.042	4.90	0.228	0.13

^a Fit of the form $\log E_p = a \log F + b$

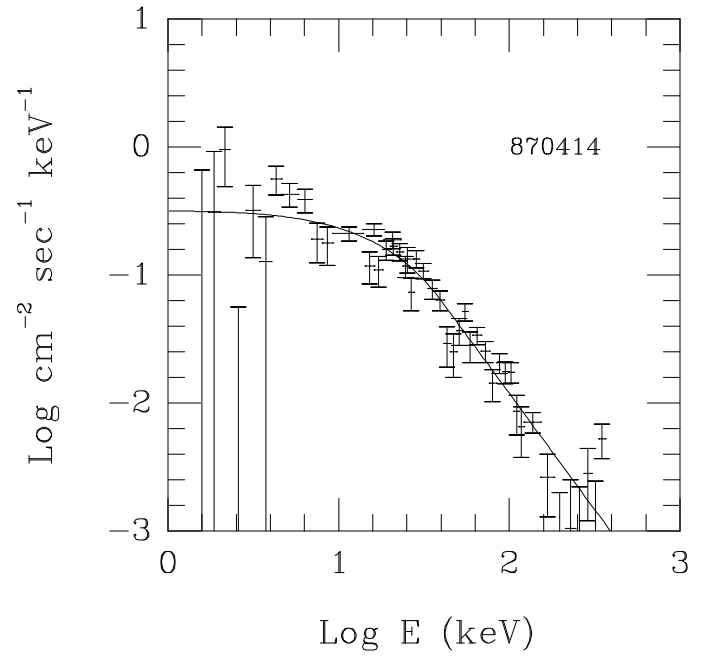
Fig. 1



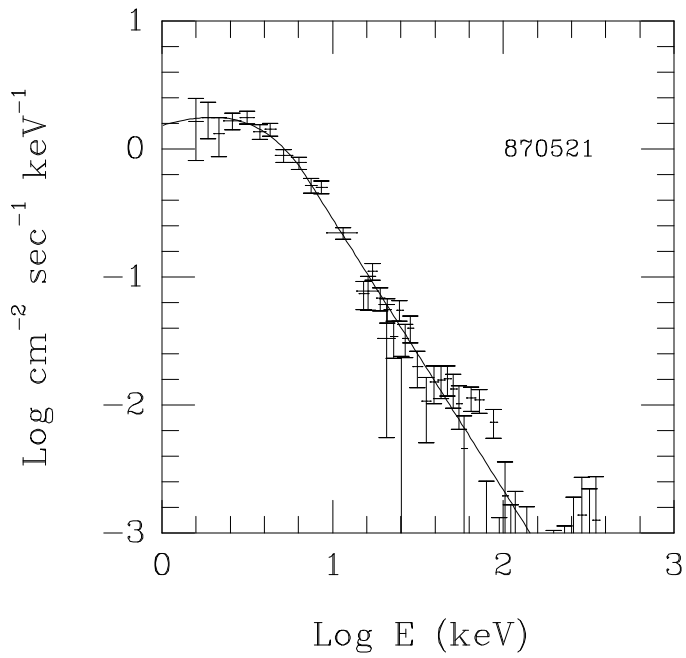
(a)



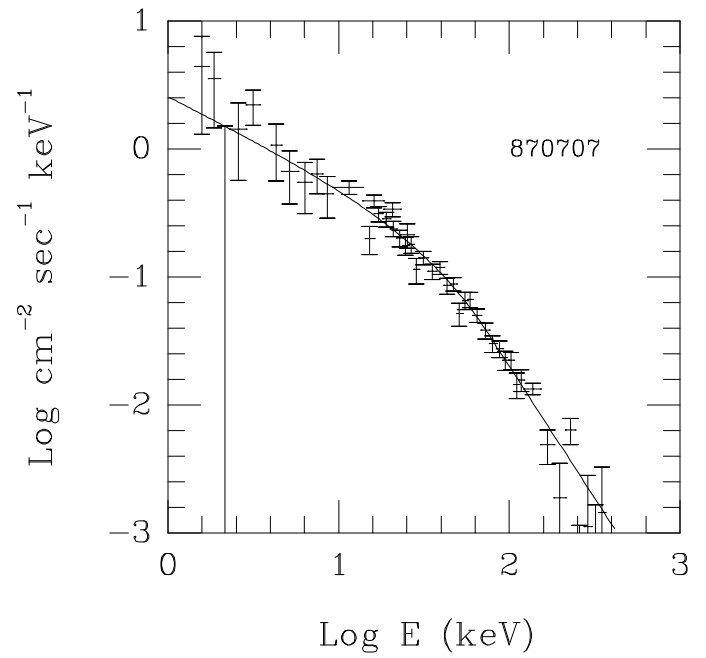
(b)



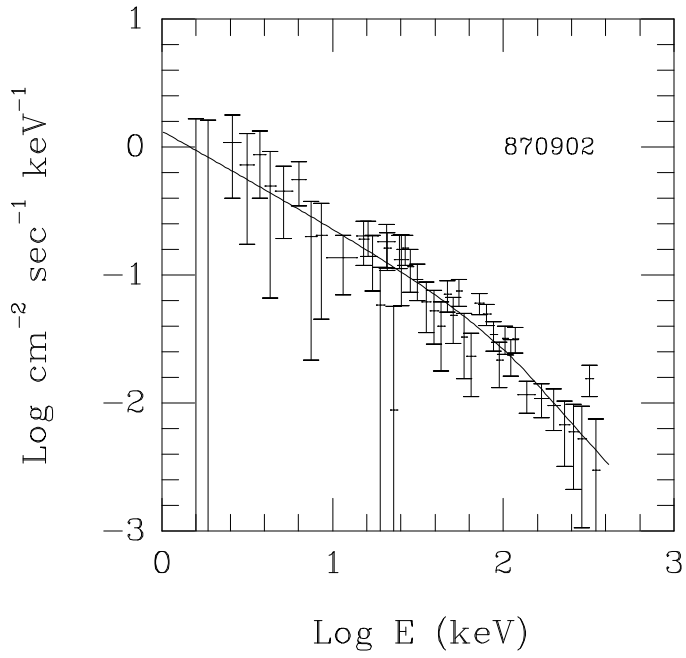
(c)



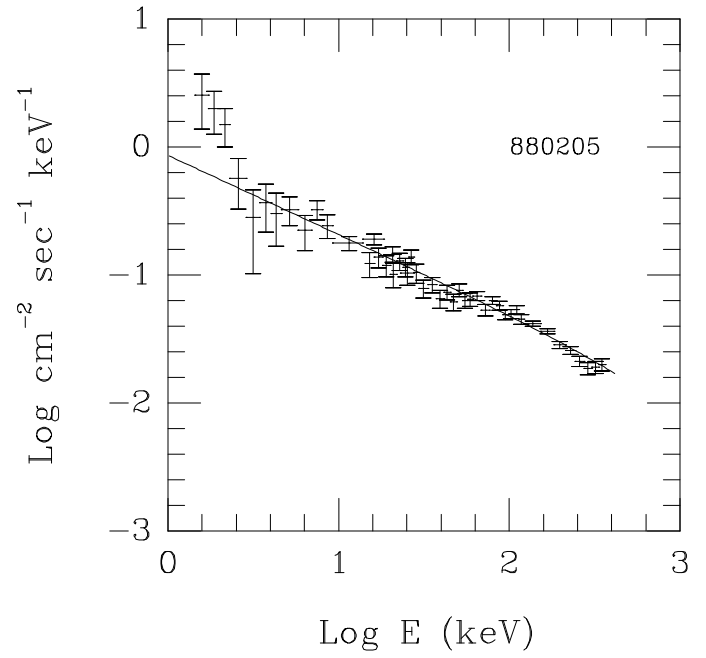
(d)



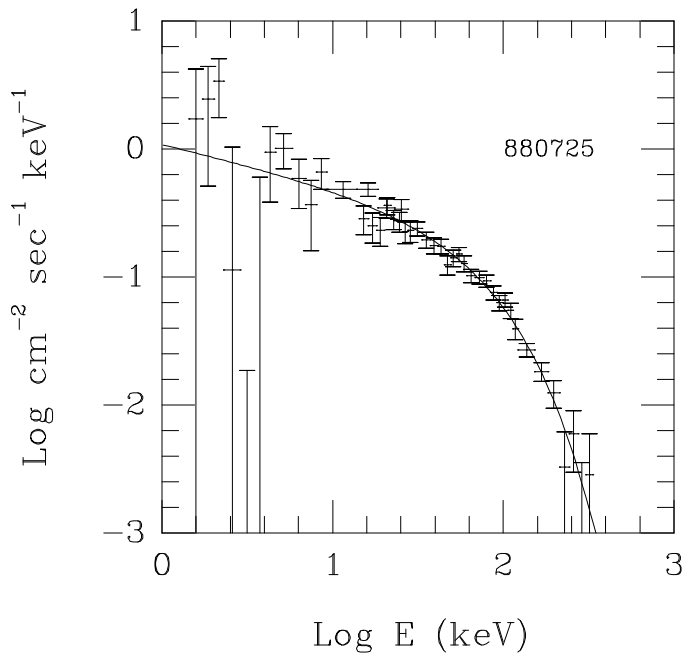
(e)



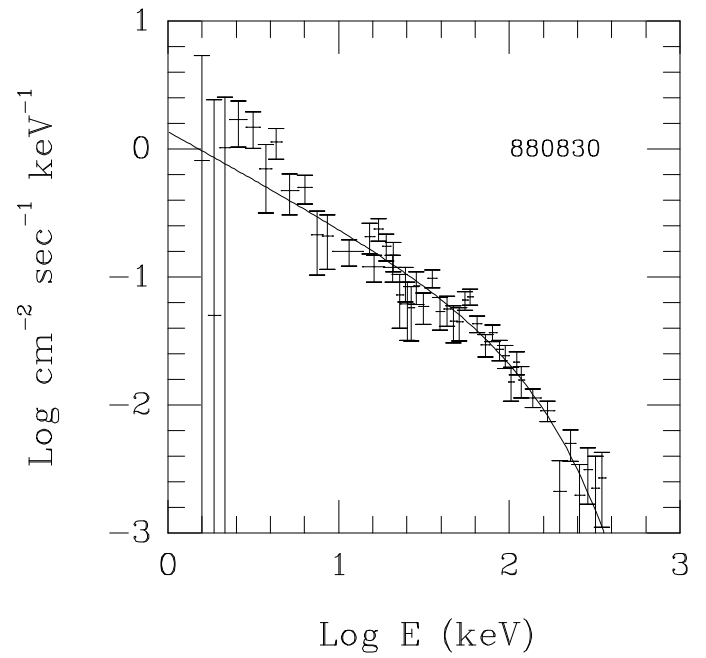
(f)



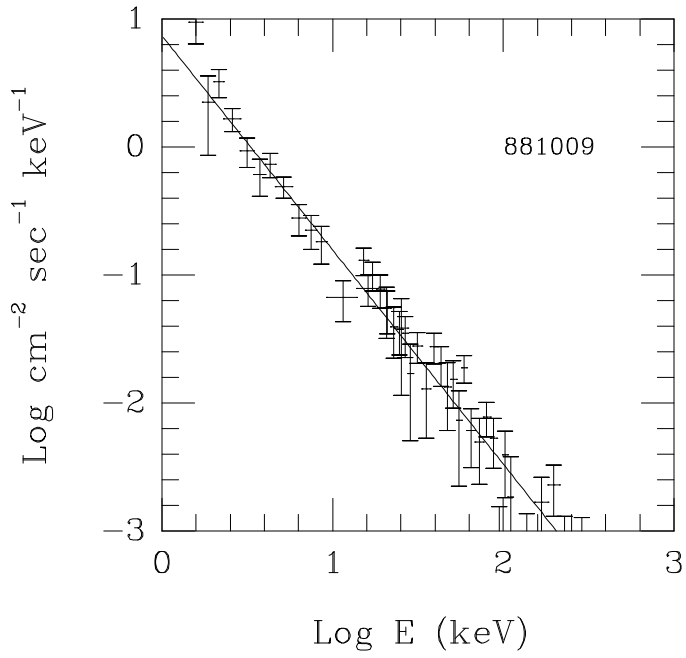
(g)



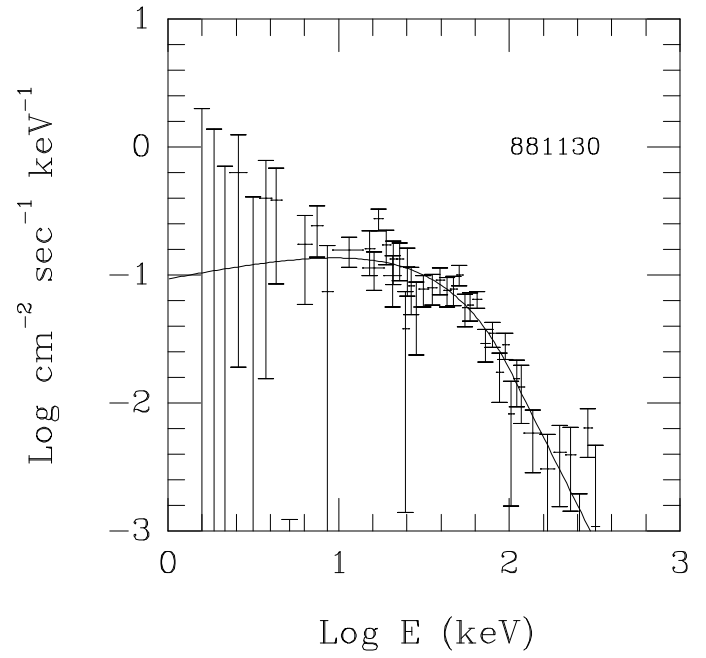
(h)



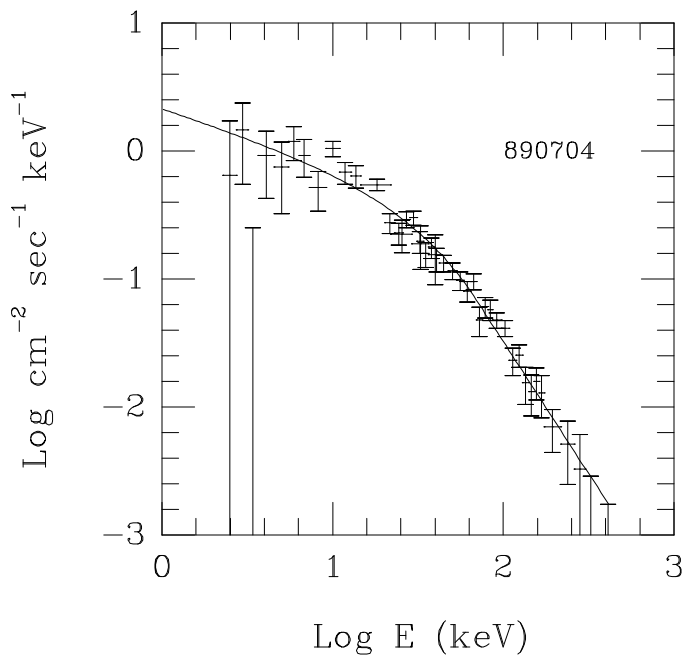
(i)



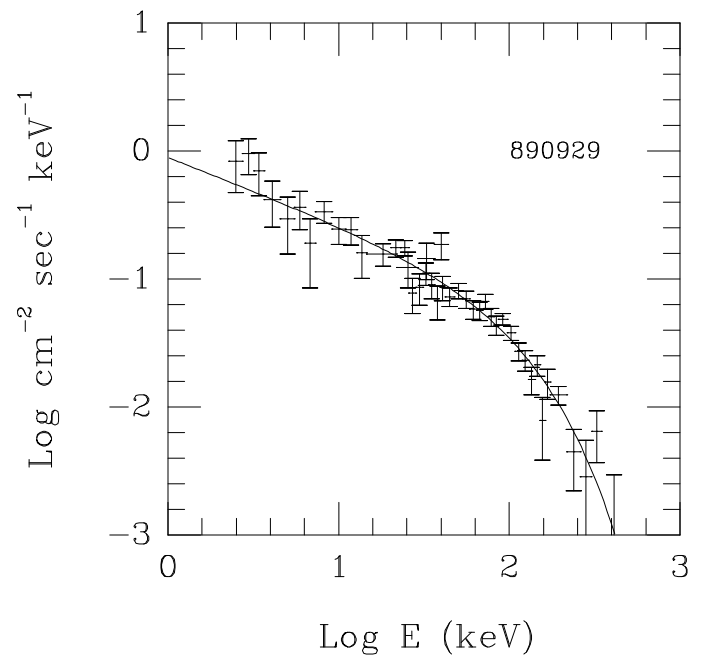
(j)



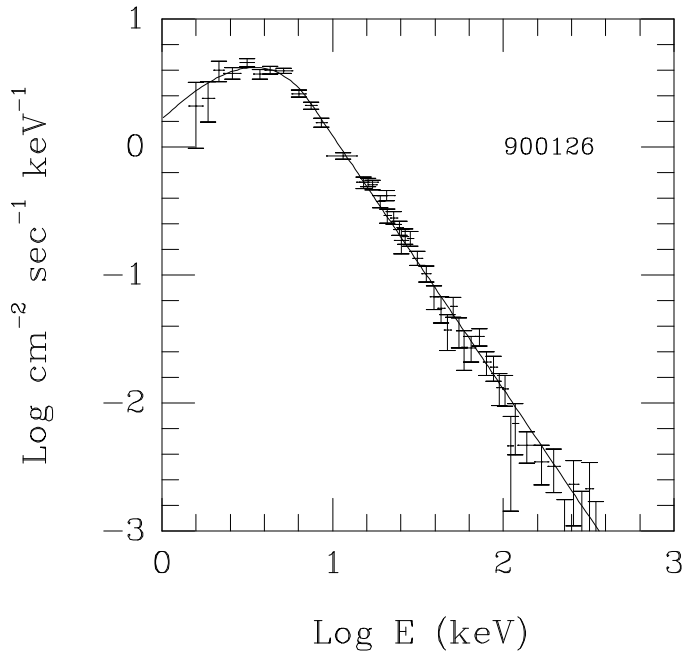
(k)



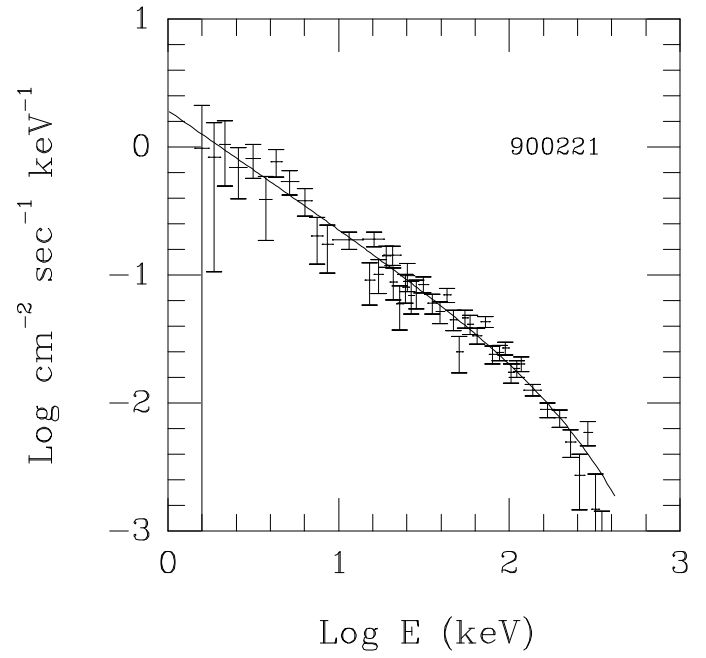
(l)



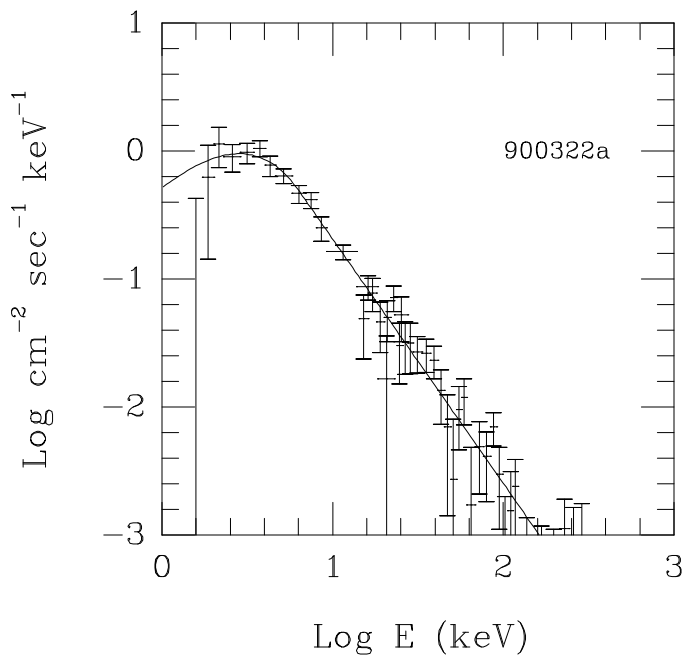
(m)



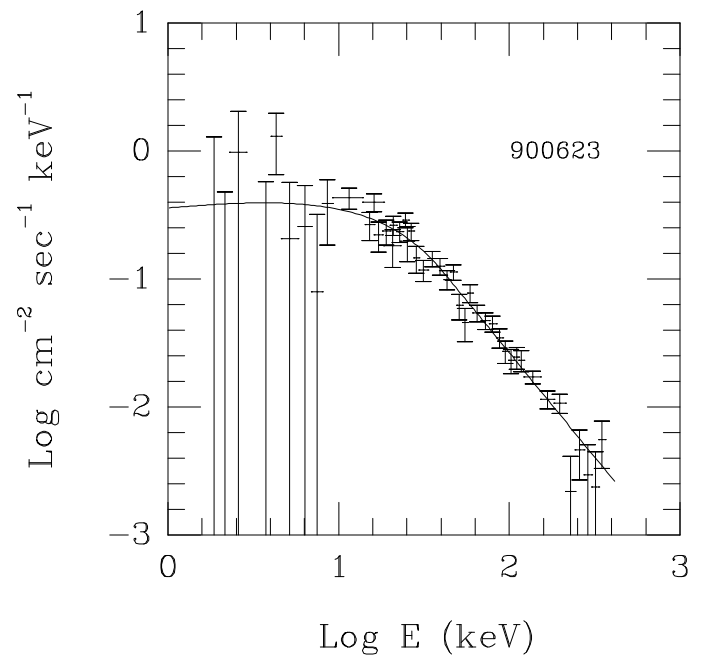
(n)



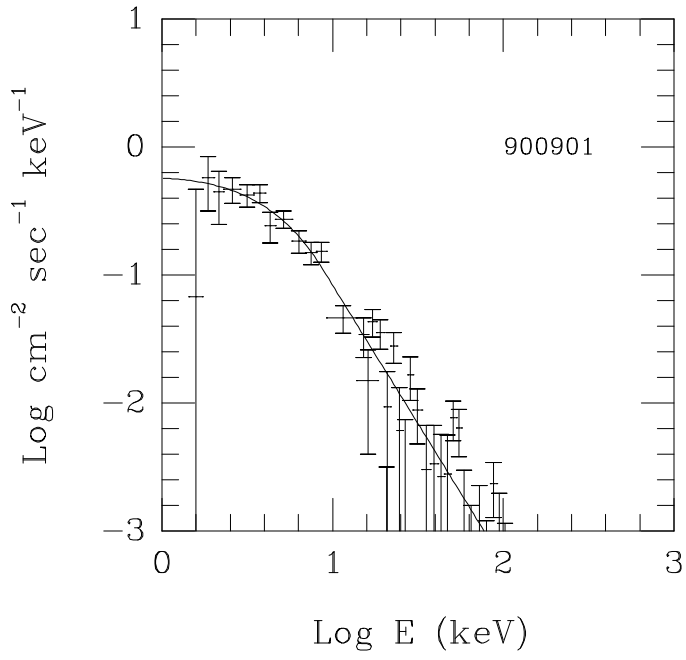
(o)



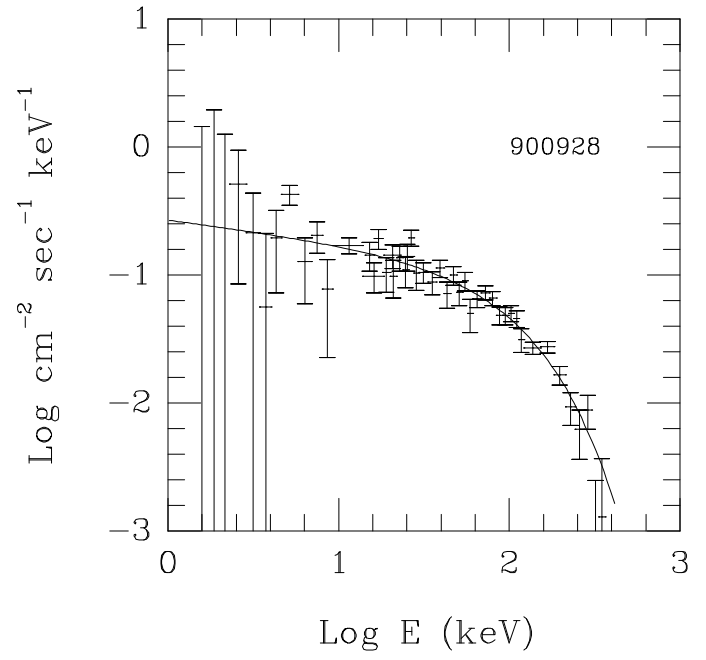
(p)



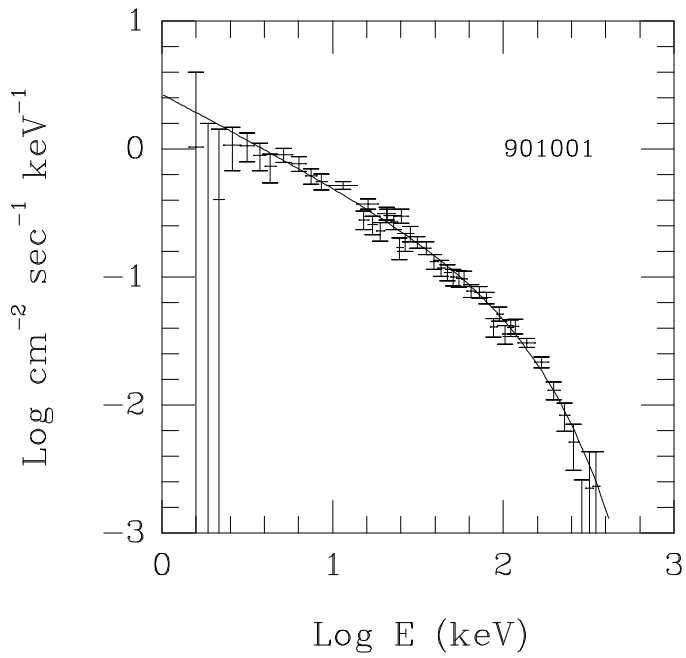
(q)



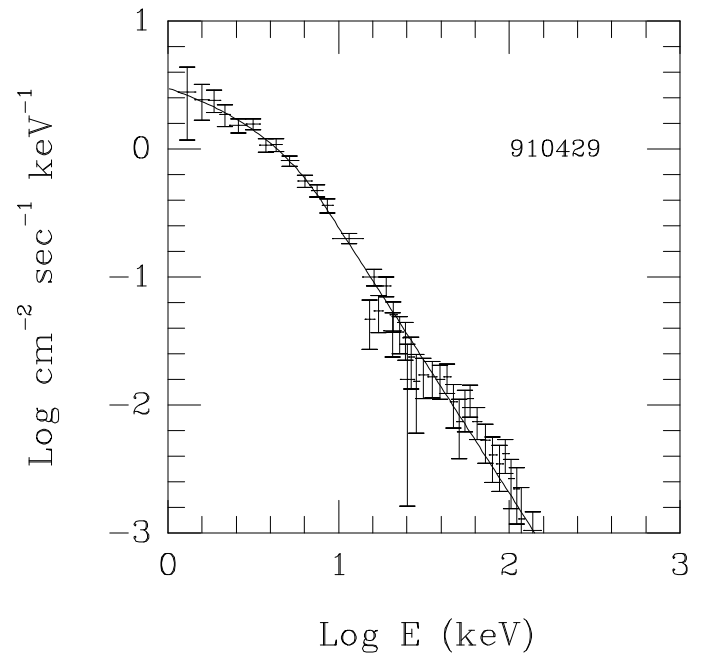
(r)



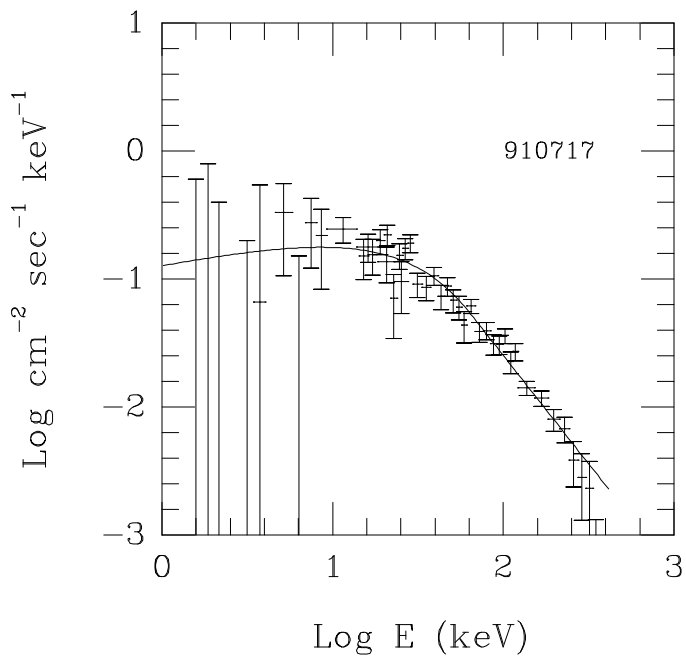
(s)



(t)



(u)



(v)

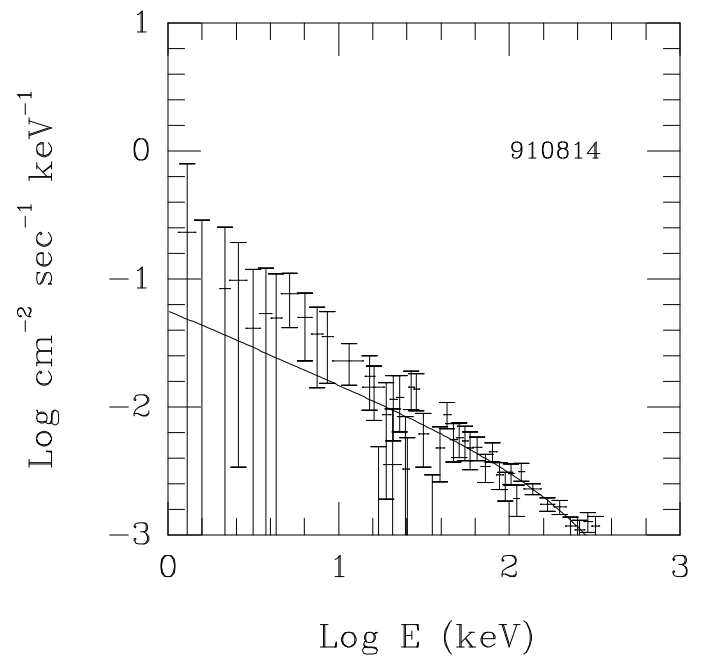


Figure 3a

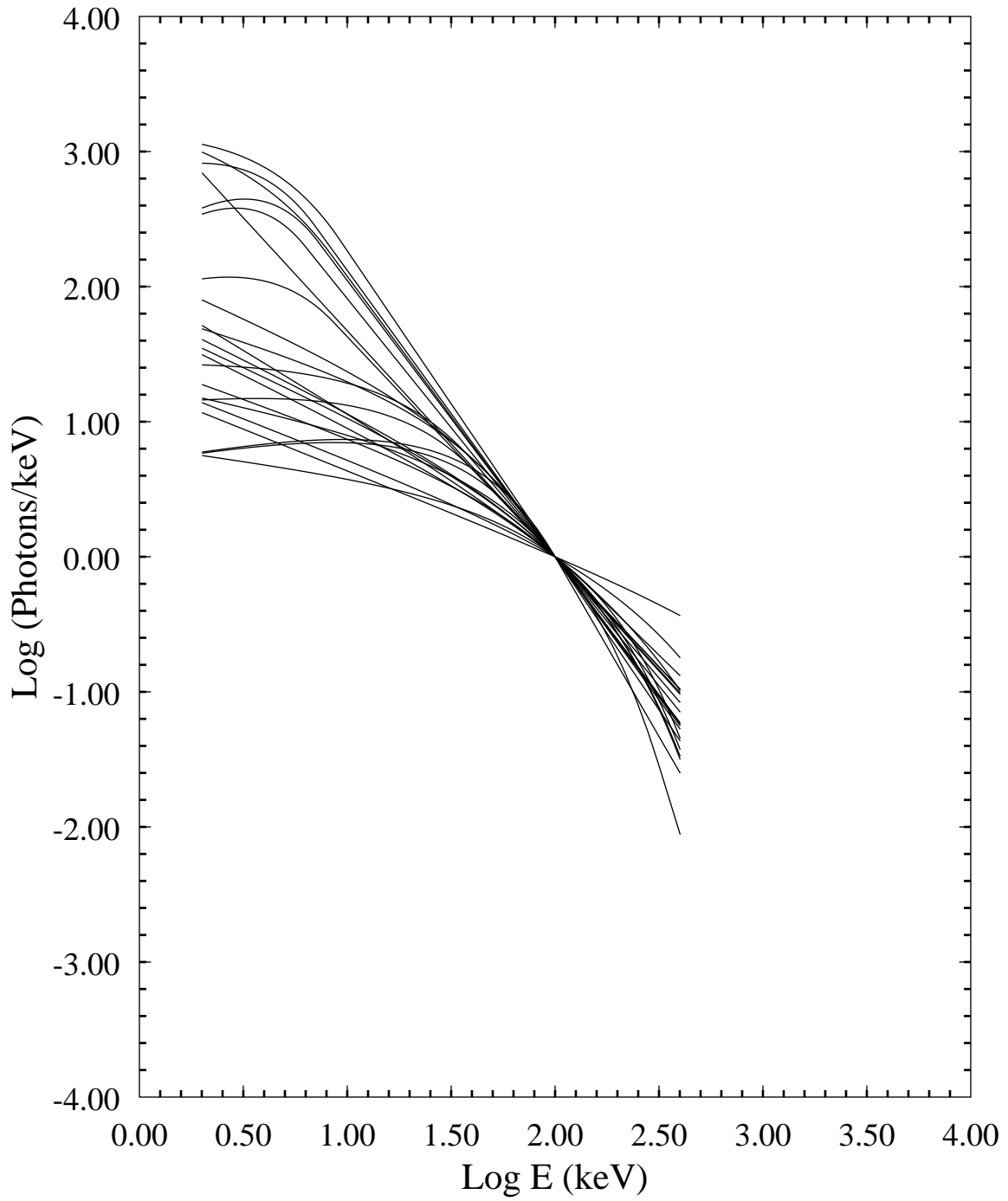


Figure 3b

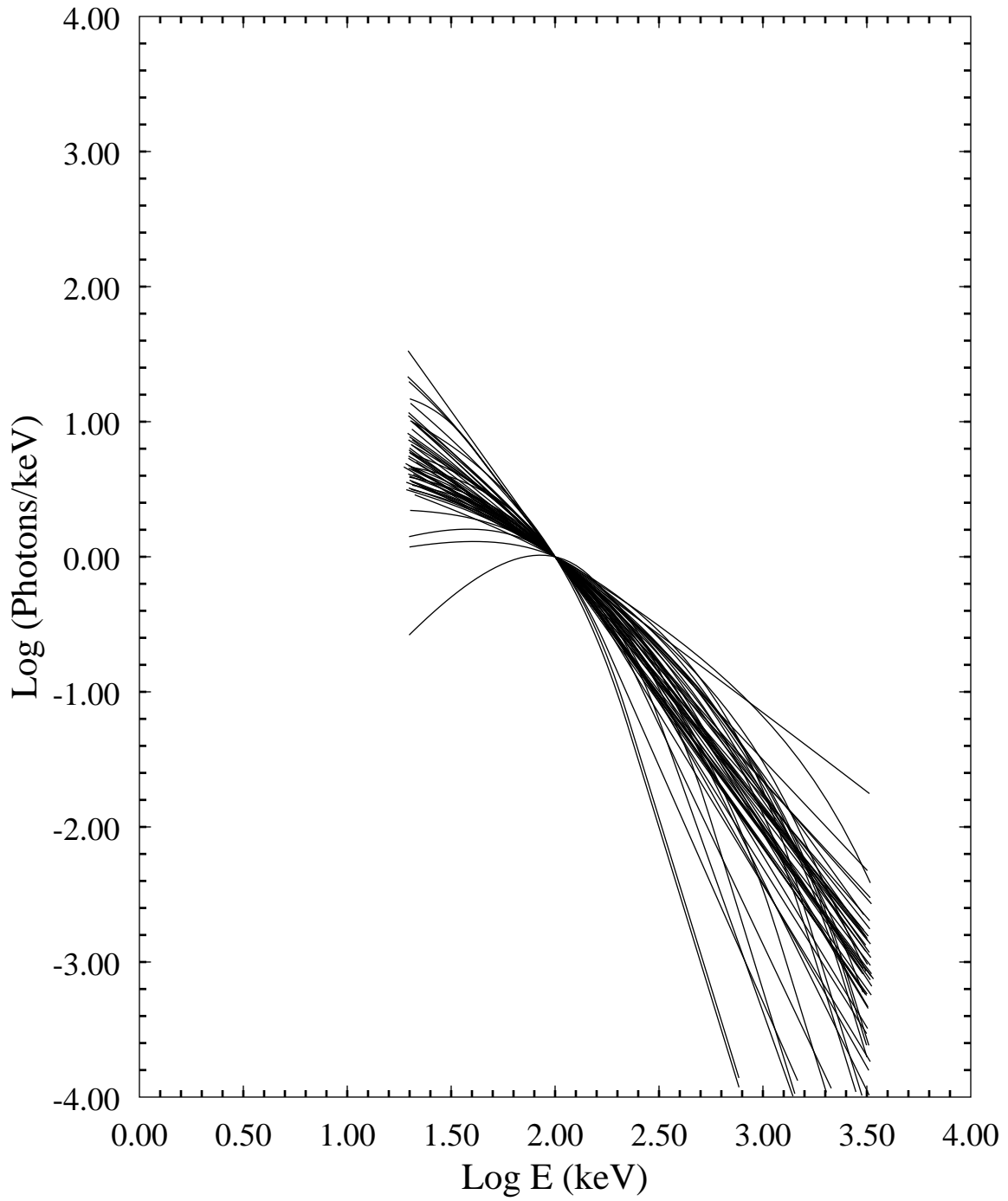


Fig 4a

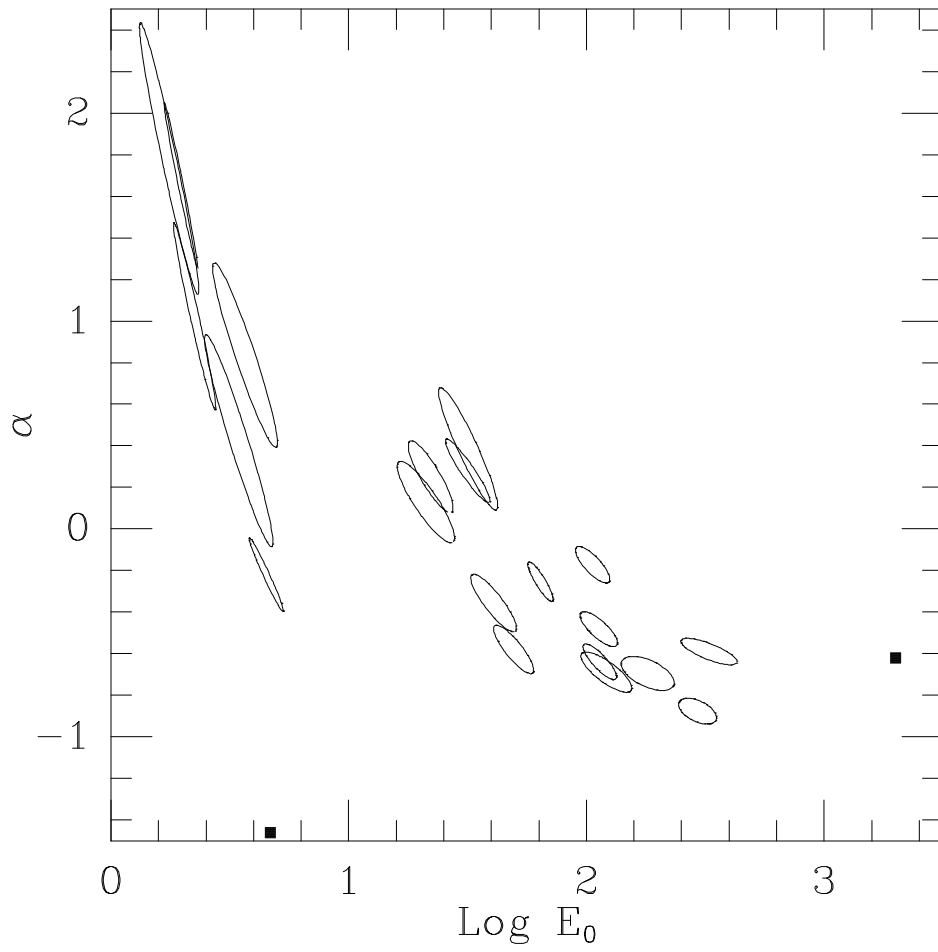


Fig 4b

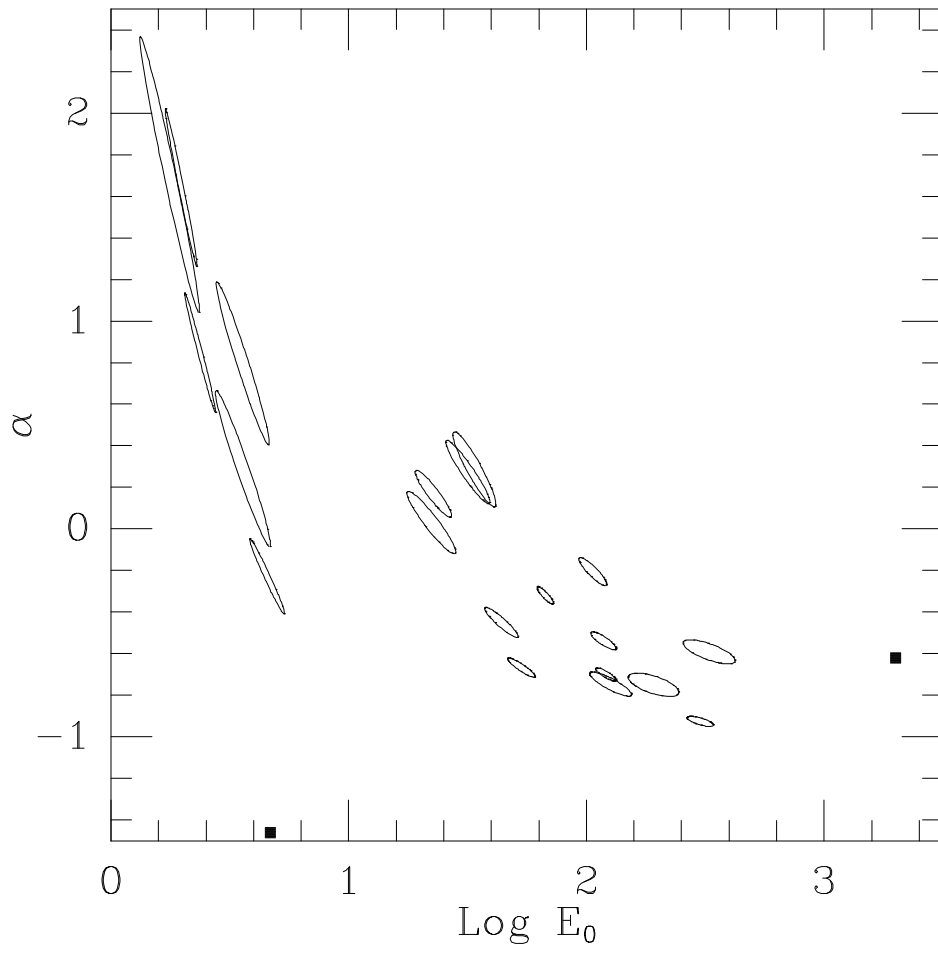


Fig 4c

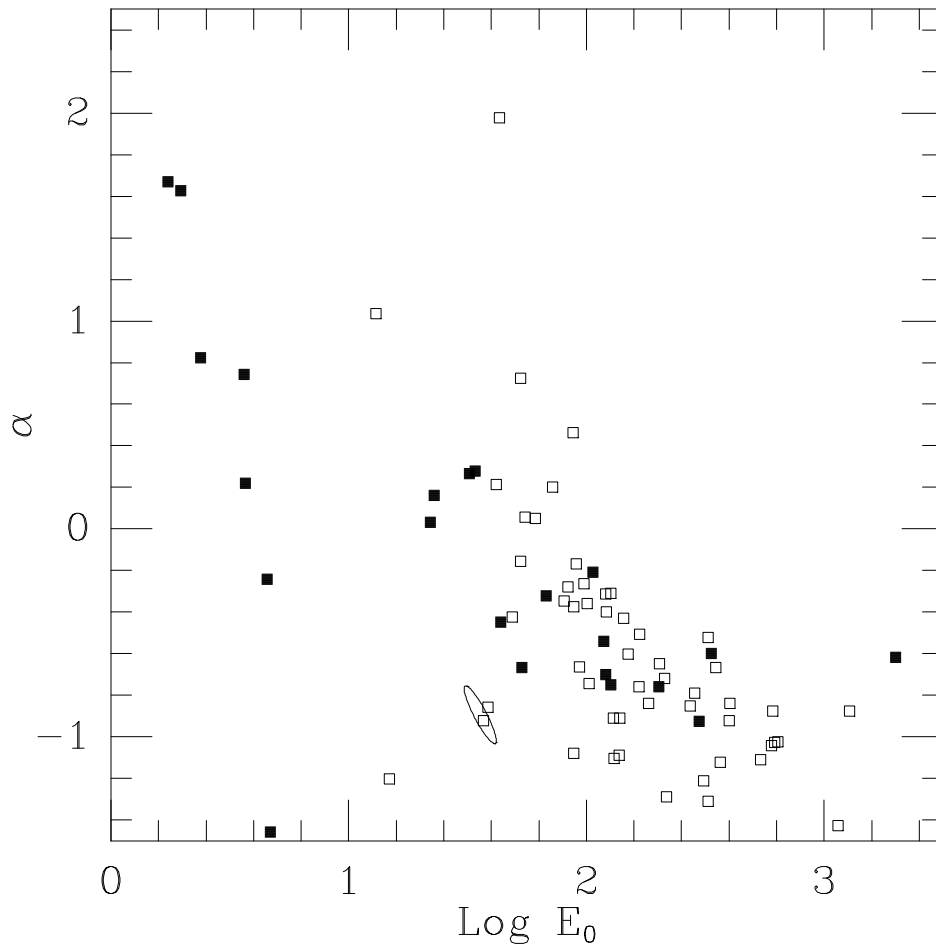


Figure 5a

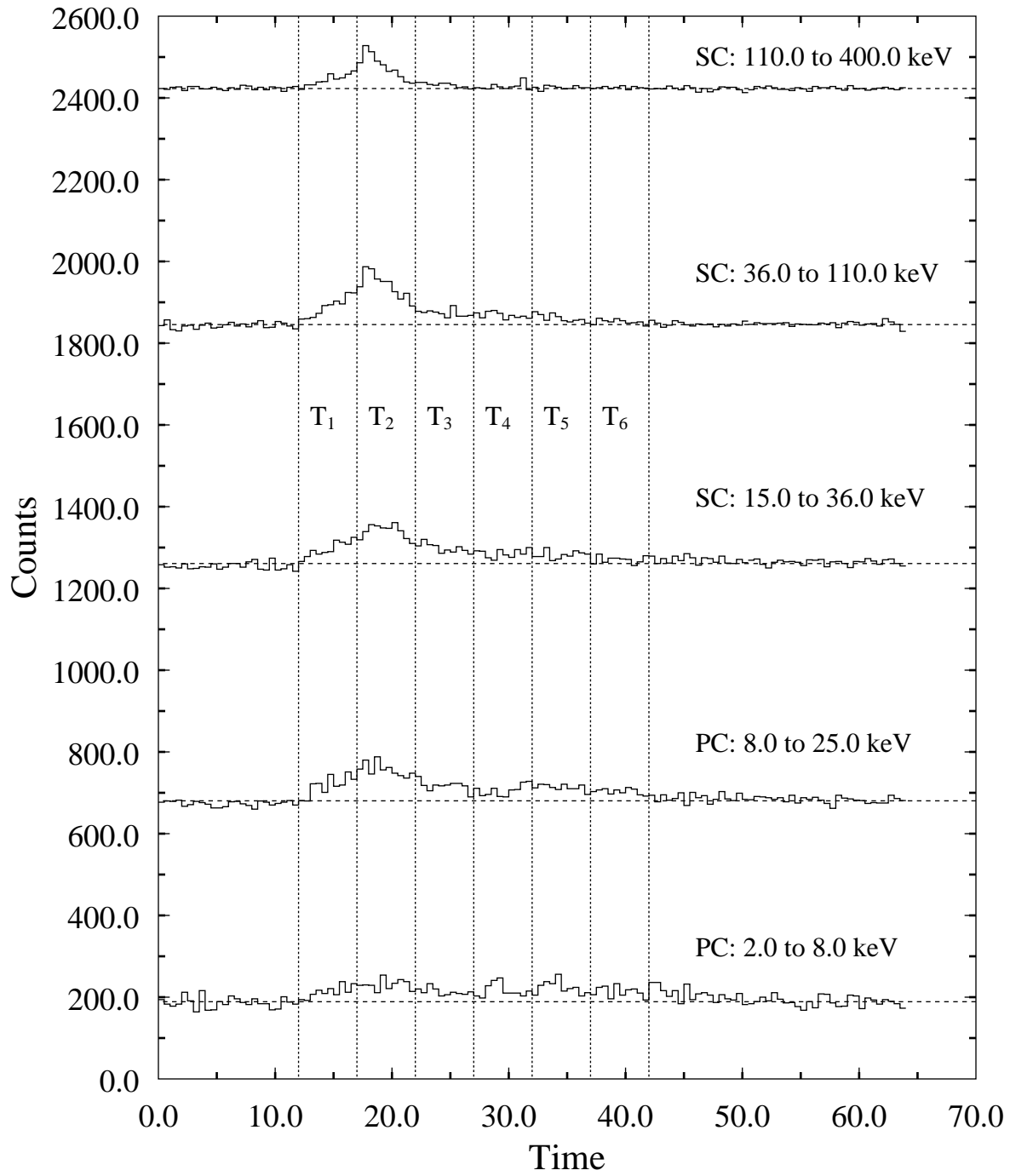


Figure 5b

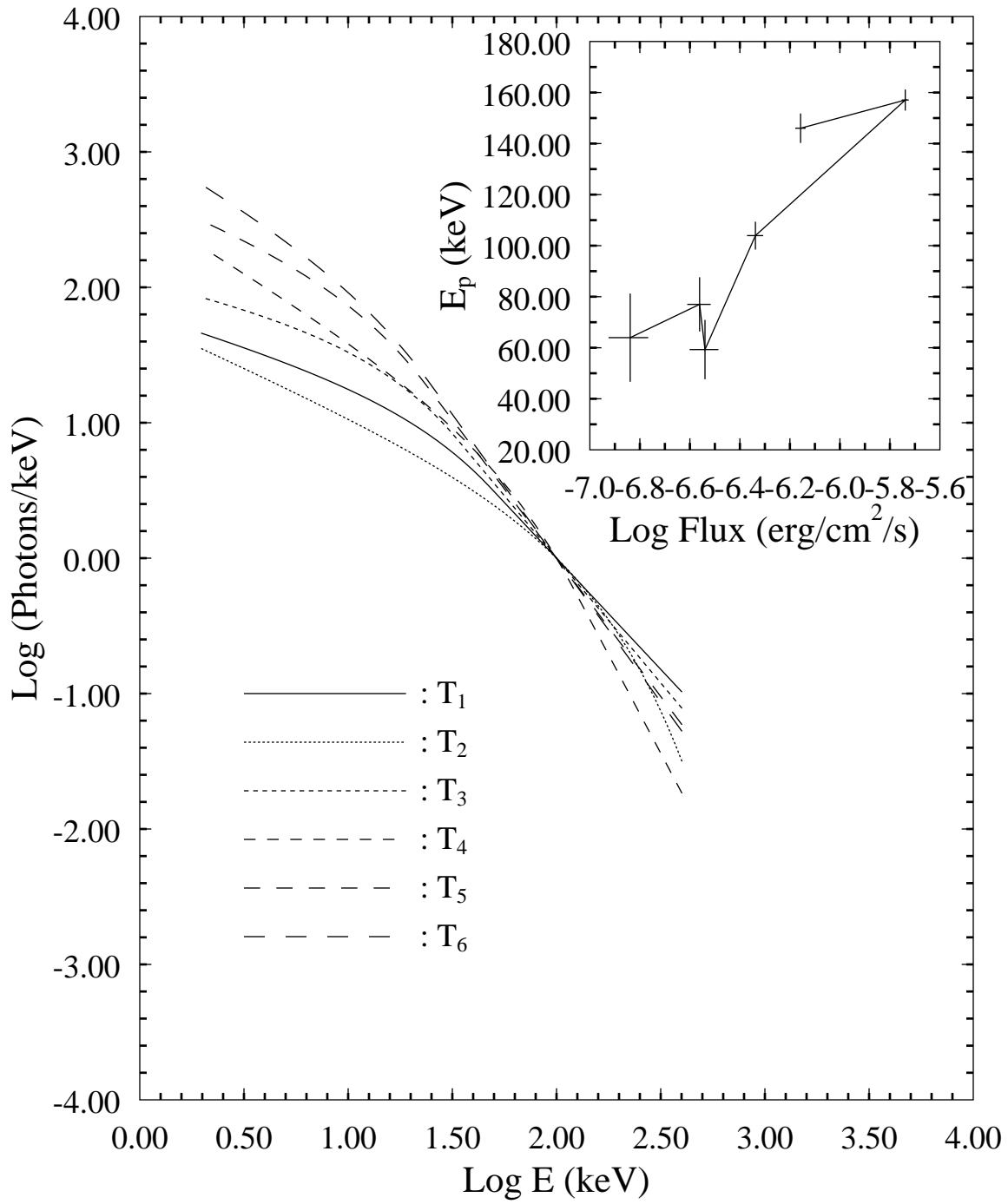


Figure 6a

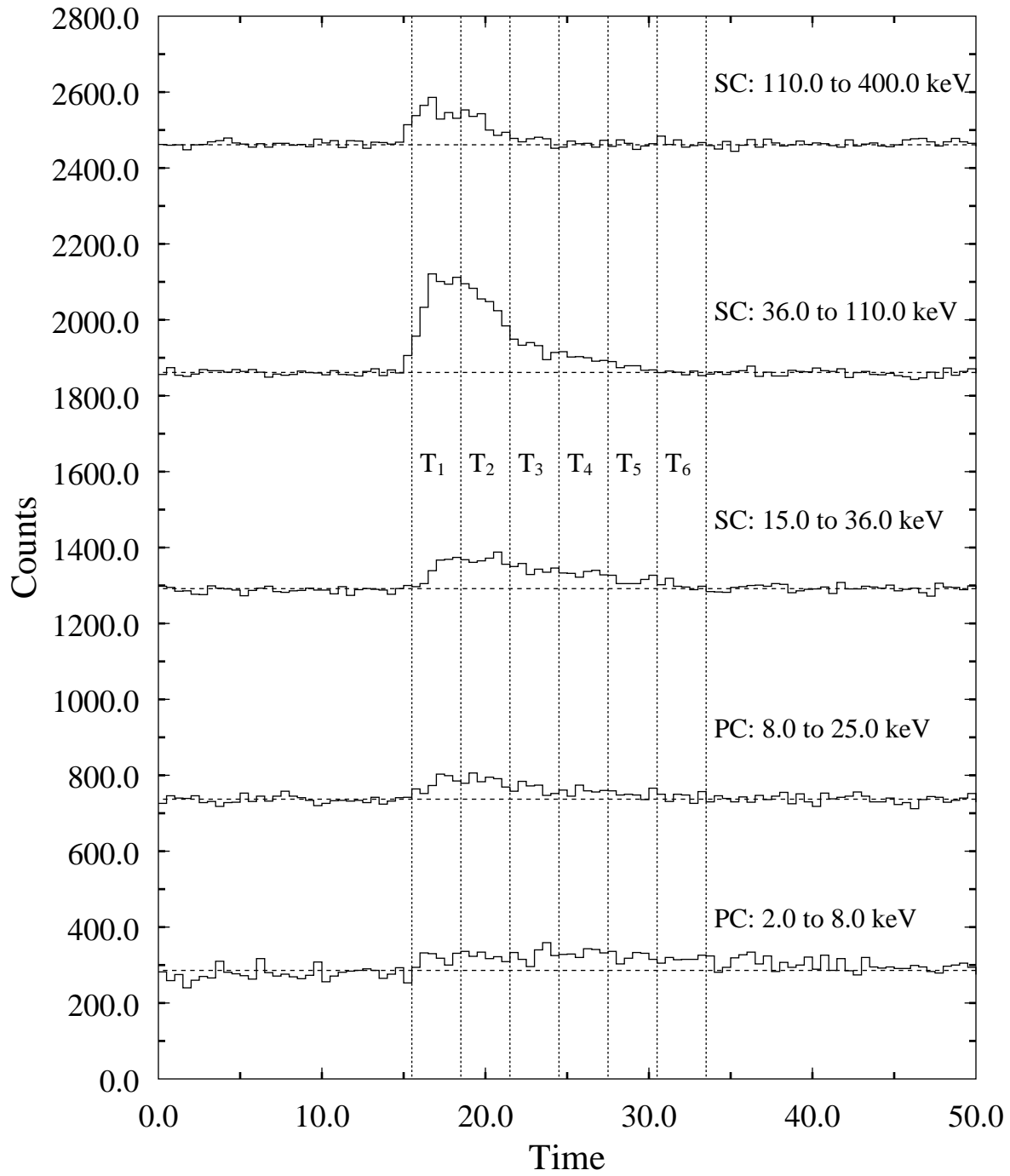


Figure 6b

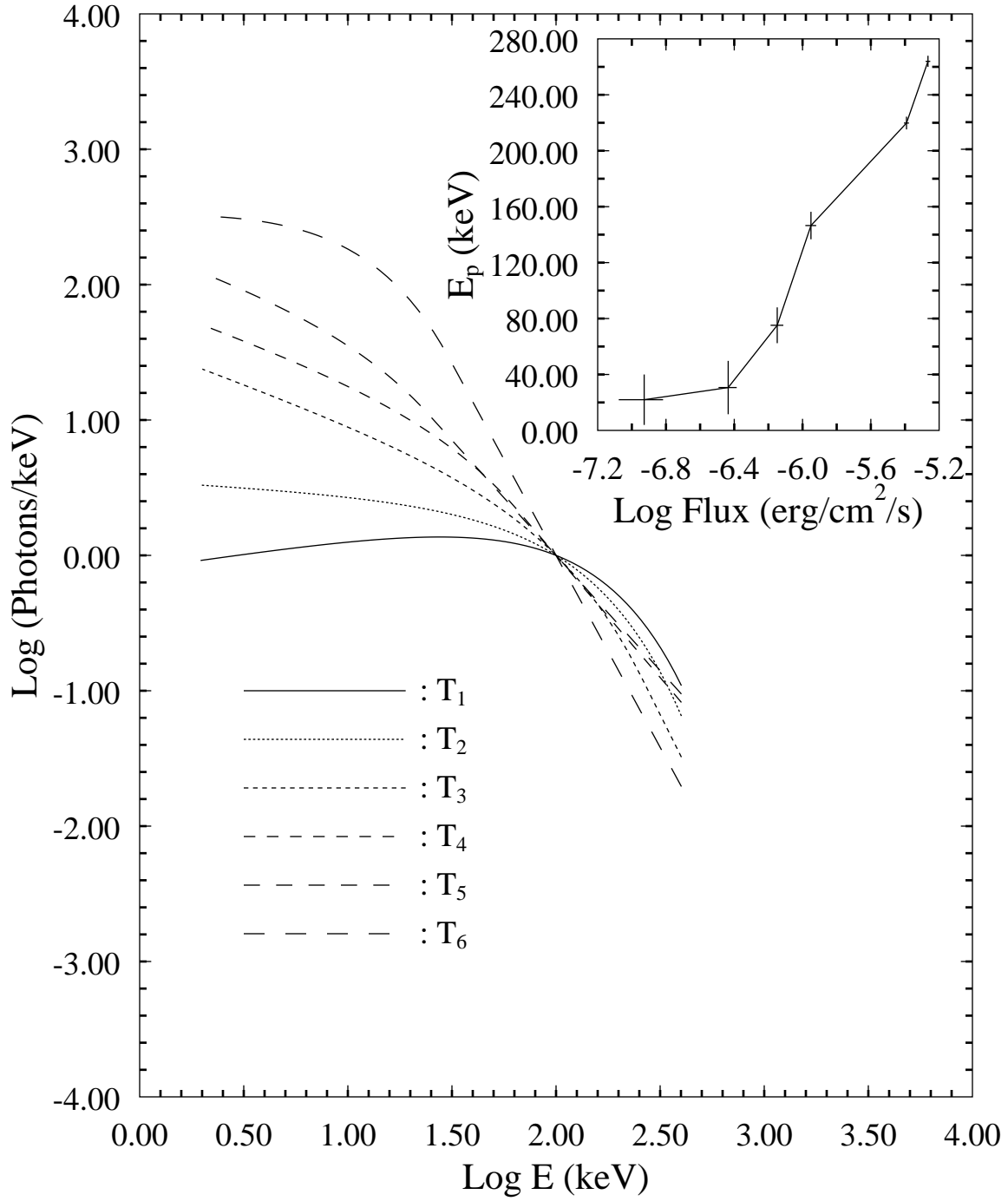


Fig 7

